Article

Not peer-reviewed version

Assessment of Soil Loss by Water Erosion at a Large Basin Scale: A Case Study of the Cheliff Basin, Algeria

Mohammed Achite , Pandurang Choudhari , Abderrezak Kamel Toubal , Priyanshu Nathawat , Nehal Elshaboury , Nikola M. Milentijević * , Tommaso Caloiero

Posted Date: 27 February 2026

doi: 10.20944/preprints202602.1876.v1

Keywords: water erosion; RUSLE; GIS; Wadi Cheliff basin; Algeria

 doi:10.20944/preprints202602.1876.v1

Article

Assessment of Soil Loss by Water Erosion at a Large Basin Scale: A Case Study of the Cheliff Basin, Algeria

Mohammed Achite [1], Pandurang Choudhari [2], Abderrezak Kamel Toubal [1], Priyanshu Nathawat [2], Nehal Elshaboury [3], Nikola M. Milentijević [4,*] and Tommaso Caloiero [5]

[1] Laboratory of Water & Environment, Faculty of Nature and Life Sciences, University Hassiba Benbouali of Chlef, P.B 78C, Ouled Fares, 02180 Chlef, Algeria

[2] Department of Geography, University of Mumbai, Vidya Nagari Marg, Kalina, Santacruz East, 400098 Mumbai, India

[3] Construction and Project Management Research Institute, Housing and Building National Research Centre, 87 El Tahrir St. Dokki, 12311 Giza, Egypt

[4] Department of Geography, Faculty of Sciences and Mathematics,University of Priština in Kosovska Mitrovica, Lole Ribara 29, 38220 Kosovska Mitrovica, Serbia

[5] National Research Council - Research Institute for Geo-Hydrological Protection (CNR-IRPI), Via C. B. Cavour, 4, 87036 Rende, Italy

* Correspondence: nikola.milentijevic@pr.ac.rs

Abstract

Water erosion is the main driver of soil loss in semi-arid mountainous regions, particularly in Algeria. Identifying the spatial distribution of erosion is a crucial first step, providing decision-makers with essential information to develop effective mitigation strategies. The main objective of this study is to apply the Revised Universal Soil Loss Equation (RUSLE) to estimate soil loss and rank the sub-basins of the Wadi Cheliff Basin (43,750 km²). Different geographical and non-spatial data sets have been employed to develop different thematic layers of the RUSLE factors such as: rainfall erosivity factor (R), soil erodibility factor (K), topographic factor (LS), crop management factor (C), and support practice factor (P). The soil erosion in the Wadi Cheliff basin in the current study ranges considerably from a minimum of 0 to a maximum of tons per hectare per year. Estimated average annual erosion rates were 0.70 t/ha in autumn 2017 and ranged between 0.00 and 0.57 t/ha in spring 2018. Information on soil erosion patterns at the sub-basin level can guide the planning of effective conservation practices. Such information is helpful for the implementation of erosion control practices and improving overall environmental management in the basin.

Keywords: water erosion; RUSLE; GIS; Wadi Cheliff basin; Algeria

1. Introduction

Soil is a natural resource made up of a thin crust layer from which over 95% of all food produced worldwide is derived [1] Soil is determinant and cross-cutting in the realization of the United Nations Sustainable Development Goals (SDGs), i.e., SDG 15.3, to a land degradation-free world by 2030. Global climate forecasts, however, show that sustained perturbation of the hydrological cycle is speeding up land degradation [2]. Therefore, this has raised the contribution of water-induced soil erosion considerably, which now accounts for 30% to 66% of all soil loss [3].

Erosion phenomena entail disaggregation, mobilization, and loss of sediment from external to the soil matrix, leading to drastic change in the surface topography [4]. Erosion of soil is a serious human and ecosystem health hazard, and it is responsible for approximately 85% of land degradation globally, covering huge expanses of land on Earth [5]. The potential increase in global soil erosion

 doi:10.20944/preprints202602.1876.v1

rate is caused by the expansion of arable land. The largest increases in erosion intensity are predicted for sub-Saharan Africa, South America, and Southeast Asia [6]. Kayet et al. (2018) approximated that an estimated 75 billion tons of soil are highly exposed annually from productive agricultural land and that it can generate economic losses of around 400 billion USD annually [7].

Soil water erosion is underlain by the intricate interaction of many factors, such as rainfall intensity, soil, vegetative cover, topography, and human activity [8]. They interact over a variety of spatial scales. For instance, high relief, high slope, and low perennial vegetative cover make the places extremely susceptible to high erosion rates [9]. Topography, vegetation, and soil type have been documented to be involved in the genesis of erosion in literature. Among them, rainfall intensity is a widespread driver, with severe rainfall events being found to be associated with high erosion rates. Besides that, topography and vegetation patterns tend to alter local rainfall distribution, affecting the process of soil erosion in turn [10,11]. The effects of water-caused soil erosion are far-reaching and widespread. The major effects are loss of fertile topsoil with resulting lower farm yields, elevated frequency and amplitude of floods through stream channel shallowing through sedimentation, and soil health impairment. Other impacts are the decline in groundwater, loss of reservoir capacity due to siltation, water quality deterioration, increased poverty levels, and loss of ecological balance [12–15].

Quantitative soil erosion rate and pattern prediction have been greatly enhanced by applying erosion modeling, conducted on different scales – small basins to the whole continents [16]. Various models were established to predict soil erosion rates, which are divided into two major categories: empirical and process-based models. Empirical models are widely applied in predicting water-induced soil loss because they are simple and require low data. Process models, however, use non-linear partial differential equations to simulate the intricate hydrology and erosion process dynamics and need extensive and intensive input data [17,18].

Some of the most well-known and widely used empirical models are: the Universal Soil Loss Equation (USLE) [19], the Revised Universal Soil Loss Equation (RUSLE) [20], and the Modified Universal Loss Equation (MUSLE) [21]. Conversely, some of the well-known process-based models include the Limburg Soil Erosion Model (LISEM) [22], the Watershed Erosion Prediction Project (WEPP) [23], the Soil and Water Assessment Tool (SWAT) [24] the Morgan–Morgan–Finney model (MMF) [25,26], the Water Erosion Prediction and Sediment Delivery Model (WATER/SEDEM) [27], and the European Soil Erosion Model (EUROSEM) [28]. Among them, RUSLE is still the most used empirical model to predict soil erosion rates since it assesses soil loss based on climatic factors and basic watershed properties [29].

Despite decades of scientific research and increasing public and political awareness, a deeper understanding of soil erosion – particularly its spatio-temporal dynamics – remains necessary to support evidence-based policy and effective land management strategies. This is particularly necessary in Mediterranean basin countries, which are extremely susceptible to soil loss under prevailing global change drivers. According to Heddadj (1997) [30] 6 million hectares of arable land in Algeria are at risk of water erosion. The amount of water lost every year from sedimentation in dams with silt-blocked silts is nearly 20 million cubic meters [31], and some erosion rates range from 2,000 to 4,000 tons per square kilometer per year [32]. Water erosion intensity differs across regions, with 47% of the western region, 27% of the central region, and 26% of the eastern region. Such alarming facts position Algeria among the most erosion-ridden countries in the world [33]. Thus, degradation of water and soil resources, as well as the environmental consequence in general, is further worsening. With the effort to mitigate these challenges, soil erosion risk mapping and assessment has become a key component of effective natural resource management and land use planning [34].

The Wadi Cheliff Basin is the largest catchment in northern Algeria, covering approximately 43,750 km². Draining into the Mediterranean Sea, it represents a major hydrological system of high agricultural significance, encompassing diverse ecosystems, numerous settlements, and extensive areas of intensive farming. Preventing further soil loss in this basin is therefore essential for regional

 doi:10.20944/preprints202602.1876.v1

water security, agricultural productivity, and environmental sustainability. Integrating the Revised Universal Soil Loss Equation (RUSLE) with geospatial tools enables accurate estimation of erosion rates and identification of erosion-prone areas. This integrated approach produces high-resolution erosion risk maps, which serve as valuable decision-support tools for land managers and policymakers, facilitating targeted land rehabilitation and erosion control measures to ensure the long-term stability of agricultural production, reservoir operation, and ecosystem functioning.

2. Materials and Methods

2.1. Study Area

The Wadi Cheliff Basin in northwestern Algeria of approximately 43,750 km² is the largest hydrological basin in the region and of special interest for environmental research. It is situated between longitudes 0°07′44″E and 3°31′07″E and latitudes 33°53′13″N and 36°26′34″N and is situated in the region of the western Mediterranean and North Africa. Its strategic location fixes its climatic and hydrologic regime, linking coastal and interior processes (Figure 1).

According to the Köppen-Geiger classification, the climate of the basin exhibits a semi-arid to arid climatic gradient from the northern lowlands southwards. Mean annual temperatures reflect the altitudinal gradient, varying from 18°C in the warmer, lower latitudes near the coast to 12°C in the cooler, higher altitudes of the south mountains. Precipitation in the basin is fairly consistent, ranging from 161 mm in dry interior regions to 662 mm in more humid, mountainous northern basins, based on long records extending from 1970 to 2018. A second characteristic of this precipitation regime is seasonality because approximately 80% of the yearly precipitation occurs between November and March. This intense seasonal focus tremendously enhances the surface run-off as well as enhancing the soil erosion enormously, particularly in instances of extensive rainfalls [35]. The geological framework of the Wadi Cheliff basin is dominated by extensive sedimentary sequences deposited from the Miocene through the Quaternary, including limestone, marl, clay, and sandstone facies, overlying older Mesozoic to Jurassic bedrock (e.g., Cretaceous clays and marls) exposed in parts of the basin margins. These lithological variations influence the soil structure, drainage patterns, and the basin's susceptibility to erosion, as carbonate-rich and fine-grained sedimentary rocks respond differently to weathering and surface runoff compared to more competent older units [36].

The hydrological environment of the Cheliff Basin is dominated by the Wadi Cheliff, Algeria's longest river and the country's main drainage system. The river is fed water by a highly complex tributary system, which flows freely when it rains, in which maximum runoff on steep mountain slopes. These conditions tend to cause flash flooding and extreme soil erosion, especially where there is heavy rain over the rugged topography of the basin. The geomorphology of the region, with a mixture of steep rocky slopes and extensive alluvial plains, adds up to irregular precipitation to enhance water-lead soil loss. Soil in the basin is extremely variable and varies from water-retentive fertile alluvial deposits in lower valleys to thin, erosive loamy and sandy soils over slopes, which is more prone to erosion under ineffective land management practices [37,38].

Land cover in the Cheliff Basin is a mosaic of rangeland, crop, and open, sparsely vegetated land, with limited isolated forest patches clinging to the more elevated topography. Steep slope agriculture, with massive overgrazing and little or no proper soil conservation measures in place, increases erosion rates, presenting extremely serious challenges to sustainable land use. The selection of such studies for this basin is governed by its highly vulnerable sensitivity towards erosive forces and the fact that there must be adequately advanced management policy that can decelerate environmental degradation [38]. While previous studies have, in particular ways, examined hydrology along with erosional processes at points of the basin, they are normally not basin wide in scope. The present study endeavors to fill this gap by proposing a conservative estimation of loss of soil due to water erosion, the spatial pattern, and the prevailing climatic control on the same. In this manner, it endeavors to provide useful advice towards sustainable water and land use and management so that this precious Algerian landscape will be preserved for the future.

 doi:10.20944/preprints202602.1876.v1

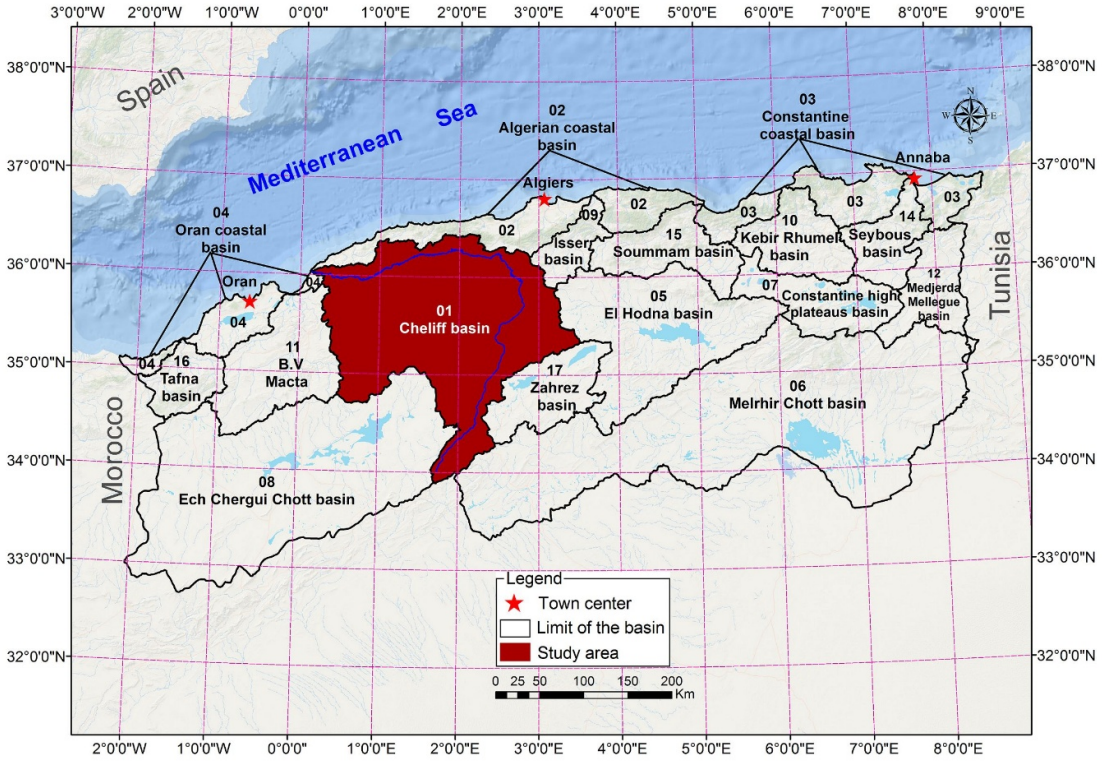

Figure 1. Location map of Cheliff Basin (Algeria).

2.2. Data

Datasets of 150 long-term precipitation records of precipitation stations from 1970 to 2018 over the WCB were accessed from the National Agency of the Water Resources (ANRH) for this research (Table 1). The records' period, however, varies in these stations as some have missing records. The selected time period of analysis is as extensive as possible considering available recorded data for most stations in the region. It is worth mentioning that the number of gaps fluctuated from 0 to 30% among all the stations in the study area. The data was subjected to quality analysis and data gaps filled with simple linear and double or multiple regressions. Collection of data was carried out through the acquisition of different types of data ranging from raster data to vector data. The raster data included climatic data ranging from 1970 to 2018, satellite images, Google Earth images, as well as Digital Elevation Model (DEM) data. The vector data included geological maps, basin area boundaries, and FAO soil data. All the data gathered were reorganized into an integrated database to ease further processing and analysis [39].

Table 1. Datasets used to calculate soil erosion.

Data type	Format	Description	Source
Rainfall data	Excel (*.xls)	Monthly and Annual Maximum daily precipitation (1970/71 – 2017/18)	Agence Nationale des Ressources Hydrauliques (ANRH)

 doi:10.20944/preprints202602.1876.v1

Topographic data (Shuttle Radar Topography Mission SRTM)	Raster (*.tif)	Resolution: 30m	United States Geological Survey (http://earthexplorer.usgs.gov/)
Satellite image Landsat 8	Raster (*.tif)	Resolution: 30m Acquisition date: (October 2017 and May 2018)	United States Geological Survey (http://earthexplorer.usgs.gov/)
Soil properties	Raster +Excel file (*.tif+*.xls)	Harmonized world soil database	Harmonized world soil database (HWSD) version 1.2 (https://www.fao.org/soils-portal/data-hub/soil-maps-and-databases/harmonized-world-soil-database-v12/en/)

Note: Datasets adopted basen on the following sources [40–42].

2.3. Methods

A widely used model for estimating soil erosion intensity is the RUSLE method, developed by the Department of Agriculture (USA) for the purpose of soil conservation and land-use planning. This method is a modification of the USLE method most commonly used to predict the average rate of agricultural land loss [19]. The Revised Universal Soil Loss Equation (RUSLE) model was employed for the purpose of research in making an estimate of the soil loss within the area under investigation. Three major steps constituted the methodology of the study, namely, data collection, processing and analysis of data, and soil loss estimation (Figure 2).

Data processing was conducted to derive the parameters required for the calculation of RUSLE factors. *R-Factor (Rainfall Erosivity)*: The factor was obtained from rainfall data daily, gap filling, and calculation of erosivity at every station [43]. *K-Factor (Soil Erodibility)*: Soil erodibility was approximated by mapping of soil textural classes and construction of textural polygons. It served to determine the susceptibility of the soil to erosion under different conditions [44]. *LS-Factor (Slope Length and Steepness)*: Slope degree, slope percentage, direction of flow, and accumulation of flow were derived from the DEM to calculate the LS factor, which is the outcome of the combined influence of both slope length and steepness on erosion [39]. *C-Factor (Cover Management)*: Land cover and land use mapping was achieved using NDVI and unsupervised classification methods. Atmospheric and geometric correction on satellite data were conducted to enhance the precision of classification [45]. *P-Factor (Conservation Practice)*: Soil conservation activities and cultural practices were evaluated with a view to including soil conservation activities as inputs for P-factor estimation.

Soil loss (A) was predicted with the RUSLE model by its factors multiplied together: R, K, LS, C, and P. GIS-based soil loss map expressed spatial patterns of erosion risk, which were easily distinguishable for highly erosion-prone sites. The map can serve as a planning and management tool for land conservation by demarcating areas that require urgent attention [39,45]. Incorporation of multi-source information and advanced GIS methods with the RUSLE model made possible the precise forecasting of soil erosion and guided strategic planning of soil conservation.

 doi:10.20944/preprints202602.1876.v1

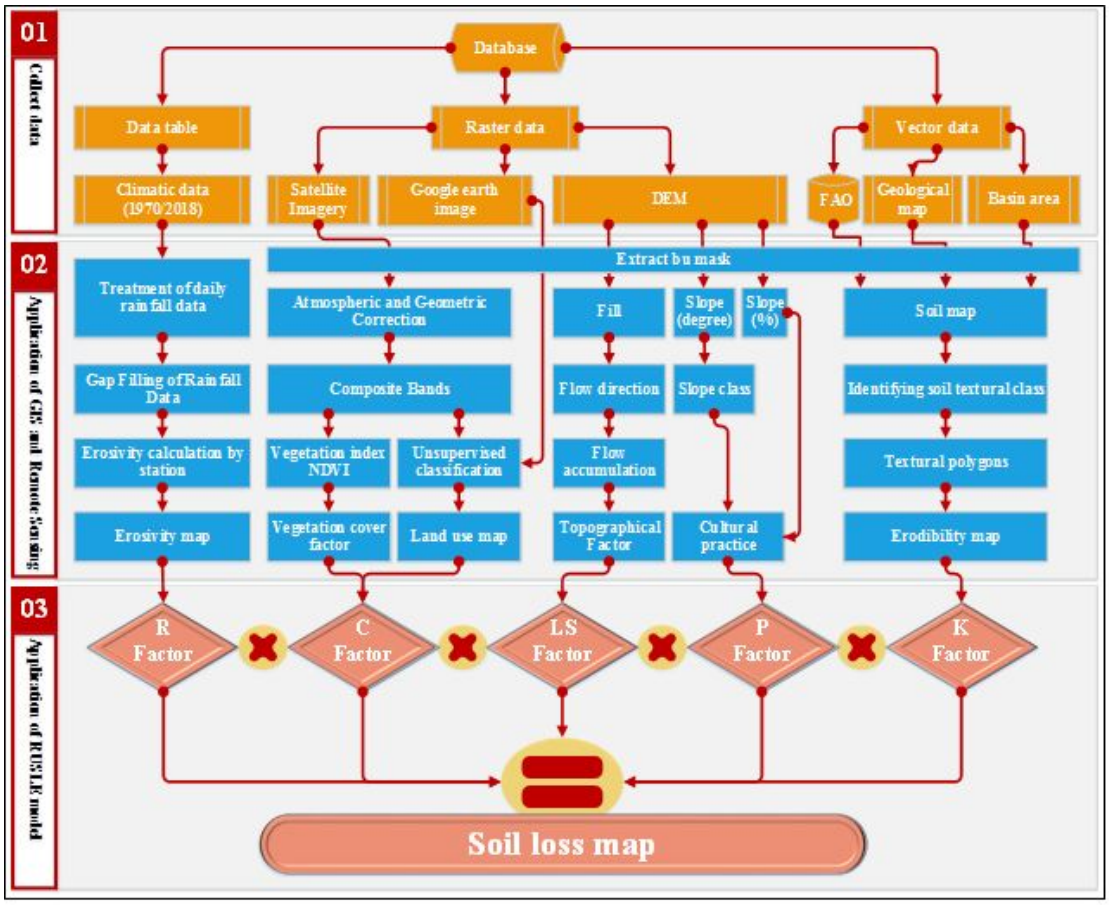

Figure 2. Conceptual flowchart of implemented methodology in the study.

2.3.1. Description of the RUSLE Empirical Model

To estimate the average soil loss, scholars utilized rainfall erosivity, soil erodibility, topographic factors (including the effects of slope steepness and slope length), land cover management, and support practices. All these factors differ significant in spatio-temporal scale and depend on the input variables taken to determine them. RUSLE is utilized to measure soil loss from erosion within each pixel. The equation is as follows:

$$A = R * K * LS * C * P \quad (1)$$

where A represents the annual soil loss rate (t ha^{-1} yr^{-1}); R denotes rainfall erosivity (MJ mm ha^{-1} h^{-1} yr^{-1}); K is the soil erodibility factor (t h MJ^{-1} mm^{-1}); LS is the topographic factor, a dimensionless value derived from slope length and steepness; C refers to the cover management factor; and P is a dimensionless factor reflecting erosion control practices such as contouring or terracing.

Because of its ability to explain many controls management methods with low data requirements, RUSLE, a variation of USLE, is a more prevalent and realistic formulation of erosion models in soil loss estimation. It is supported by the argument that sediment transport regulates soil detachment from a slope or plot and deposition [46].

2.3.1.1. Rainfall Erosivity Factor (R)

The R factor plays a significant role in determining soil loss rates, as it directly contributes to sheet and rill erosion caused by raindrop impact and surface runoff [47–49]. Erosion risk increases with higher rainfall intensity and longer storm duration [50].

 doi:10.20944/preprints202602.1876.v1

In this study, rainfall erosivity (R) was estimated using the empirical model proposed by [51] which expresses *R* (in MJ mm ha^{-1} h^{-1} yr^{-1}) as:

$$R = b_0 . P' . \sqrt{d}(\alpha + b_1 . L) \quad (2)$$

Where, b0 represents a constant value of 0.117 MJ mm ha-1 h-1, while b1 is defined as - 0.015 d0.5 mm-1.5, and the parameter α is expressed as 2.00 d0.5 mm-0.5. Here, L corresponds to the longitude of the site, P′ denotes the total annual precipitation in millimetres, and d signifies the maximum daily precipitation (in mm d-1) averaged over multiple years.

R-values were calculated for 150 precipitation gauge stations distributed across the basin. These point-based estimates were then spatially interpolated using the inverse distance weighting method to generate a continuous map of rainfall erosivity across the study area.

2.3.1.2. Soil Erodibility Factor (K)

Soil erodibility factor (K) is a quantitative indicator that serves as a measure of soil susceptibility to erosion through precipitation and runoff. It is an empirical measure that indicates the characteristic texture of the soil. Soil texture is a major factor which influences the intensity of soil erosion, along with its structure, organic matter content, and water permeability [49]. The soil erodibility factor, K, used in this paper is taken from the Harmonized World Soil Database (HWSD) version 1.2.

2.3.1.3. Topographic Factor (LS)

The topographic factor (LS) consists of two elements: a slope gradient factor (S) and a slope-length factor (L), both derived from the DEM. To determine overland flow (surface runoff), slope-length and gradient parameters play an essential role in soil erosion models [52]. The LS factor was calculated using the equation proposed by Moore and Burch (1986) [53], which has been widely adopted in various studies, including Markose and Jayappa (2016) [50]:

$$LS = \left(\text{flow accumulation} \times \frac{\text{Cell size}}{22{,}1}\right)^{0,4} \times (\sin \text{slope} \times 0.0896)^{1.3} \quad (3)$$

2.3.1.4. Crop Management Factor (C)

The C factor or crop management factor is the relation of cultivated land loss of soil to the equivalent clean-tilled continuous fallow under certain conditions. Certain factors affect it, such as specific vegetation cover, rotation pattern, overall management operations, and the falling precipitation distribution over clear-cut crop vegetative periods [54]. Based on Panagos et al. (2020) [55] revealed that following the topography, the second most significant factor in soil erosion hazard regulation is vegetation cover.

The Normalized Difference Vegetation Index (NDVI) has been widely utilized in developing methodologies for estimating the C factor, as demonstrated in previous studies [e.g. 55,56,57,58]. In this study, remote sensing techniques were applied to determine land use within the study area using the following steps:

Reflectance values were extracted from Landsat OLI imagery,

Sun-angle corrections were applied to the reflectance values, and

NDVI was computed using reflectance from Band 4 (red, R_4) and Band 5 (near-infrared, R_5), following the standard formula [50]:

$$C = \exp\left[\frac{-\alpha NDVI}{\beta - NDVI}\right] \quad (4)$$

where C is the plant cover factor; NDVI = (R5-R4)/(R5+R4); α and β are coefficients (α=2 and β=1) [59].

2.3.1.5. Conservation support practice factor (P)

 doi:10.20944/preprints202602.1876.v1

The P factor measures the impact of these practices by dividing the soil loss from straight-line farming on the sharpest slope from upstream to downstream by the soil loss from a support activity. Cross-cropping, contour cropping, and strip cropping are the most widely utilized farmland support techniques [60–62]. According to Panagos et al. (2015) [55] the P factor is locally computed in this study as a function of slope (Table 2).

Table 2. P-factor values.

Slope (%)	P value
9–12	0.6
13–16	0.7
17–20	0.8
21–25	0.9
> 25	0.95

Source: Authors defined values based on Panagos et al. (2015) [55].

2.3.1.6. Soil Loss Factor (A)

Five raster layers (*.tif) were developed for the five components R, K, LS, C, and P. Soil loss across the Wadi Cheliff basin was estimated by applying the RUSLE equation, where the values of each factor were calculated on a pixel-by-pixel basis and multiplied accordingly for every pixel within the study area.

3. Results

The DEM of the region illustrates the hydrographic network and topography from -4 m to 1969 m. Rain gauges (circles with the right half black), sub-basins (black outlines), and wadis (blue lines) are indicated by the legend (Figure 3). The elevation is high (1969 m) in the northern and central areas, decreasing to -4 m in the south. Major wadis like Wadi Cheliff, Wadi Rhoudia, and Wadi Sakki form a tight hydrographic system, draining water southwards. Rain gauges like those at Sidi Belkacem and El Malah are well-positioned for precipitation measurement. Sub-basins like Wadi Touil and Wadi Soussea are painted black, marking drainage areas. DEM strengthens hydrology analysis, as testified by Tarboton (1997) [63], yielding critical information on water resource distribution.

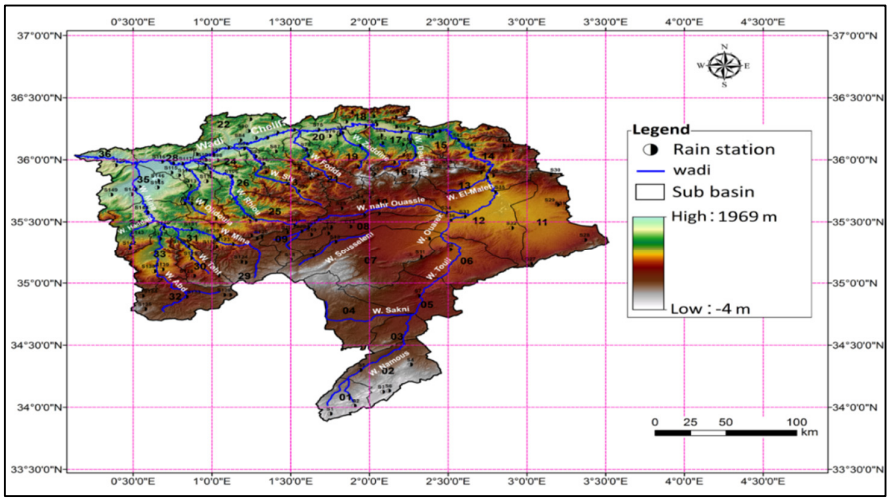

Figure 3. Digital elevation model (DEM) of the study area. The rain gauges (*circle with right half black*) and the hydrographic network (*blue lines*) are also reported.

 doi:10.20944/preprints202602.1876.v1

The DEM map of the area under study traces topography according to elevation ranges of 200 m, starting from below mean sea level (-4 m) to 1969 m. The legend marks wadis (blue lines), basin limit (white border), and elevation bands: -4 to 200 m (light blue), 200-400 m (light green), 400-600 m (green), 600-800 m (dark green), 800-1000 m (yellow), 1000-1200 m (orange), 1200-1400 m (red), 1400-1600 m (dark red), 1600-1800 m (brown), and 1800-1969 m (light yellow) (Figure 4). Northern parts close to the Mediterranean Sea, such as Wadi Cheliff, have elevations of -4 to 400 m, changing to higher elevations (600-1000 m) in the middle. Southern and eastern regions, covering Dahra Valley, have elevations of up to 1969 m. Wadis drains water through different terrains, facilitating drainage. This DEM facilitates hydrological modeling, as noted by Tarboton (1997) [63], to offer essential information on elevation-based water flow and resource management.

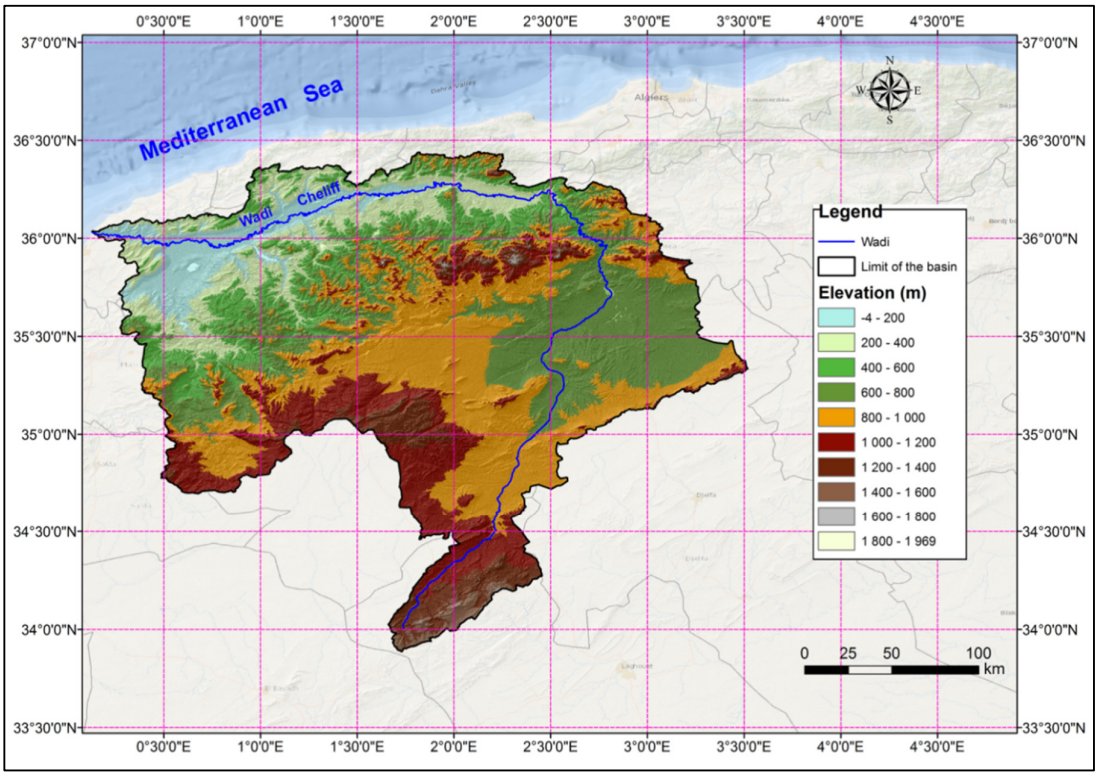

Figure 4. DEM of the study area represented in elevation classes of 200 m. The first elevation class also includes areas below mean sea level, while the highest elevation (1969 m) is the upper limit of the largest class.

The slope map of the study area represents terrain steepness, divided into classes (Table 3): 0-3%, 3-12.5%, 12.5-25%, and >25%, and is demarcated by basin boundary in white (Figure 5). Legend 0-3% slopes (yellow) covering an area of 10,033.62 km² (22.93%), which primarily represents northern plains near the Mediterranean Sea, for instance, Wadi Cheliff. The class 3-12.5% (orange), covering an area of 19,929.91 km² (45.55%), dominates central parts. Steep slopes of 12.5-25% (brown) occur at 8,452.62 km² (19.32%) and >25% (dark brown) at 5,334.35 km² (12.20%) and are in the highlands in the south and east, for instance, Dahra Valley. This distribution makes it possible to study erosion and hydrology, asserts Moore et al. (1991) [64] which highlights varied land use potential within the area.

 doi:10.20944/preprints202602.1876.v1

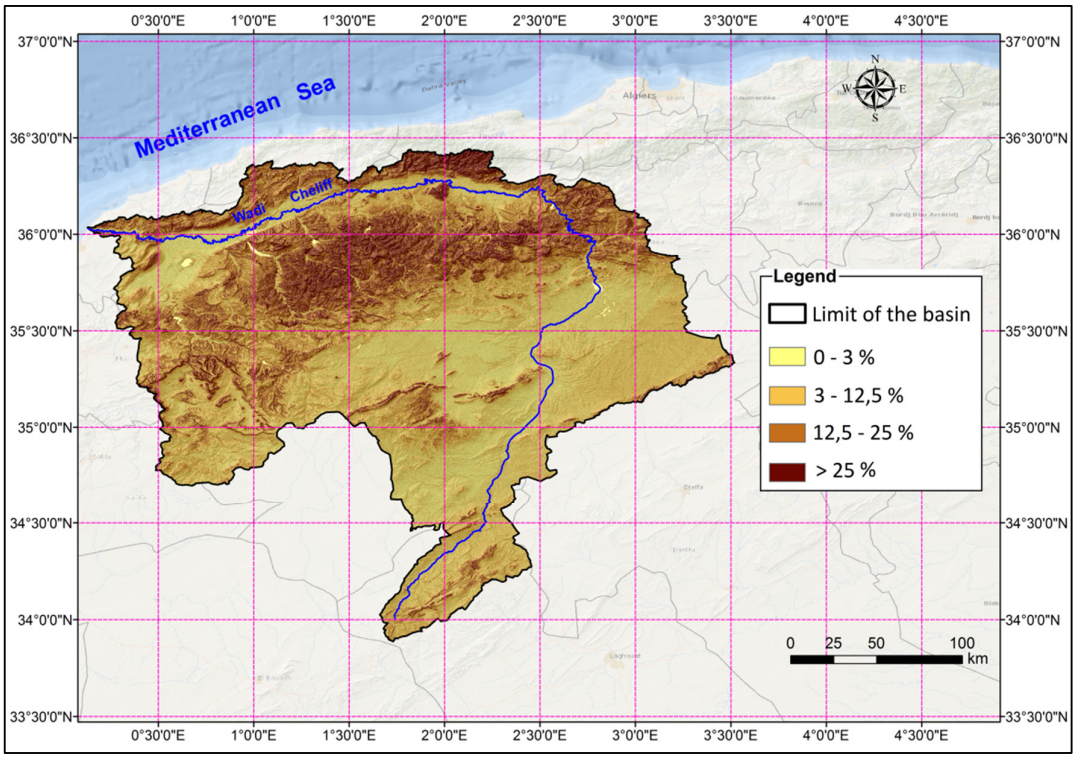

Figure 5. Slope map of the study area.

Table 3. Classes in percentage of the slope map.

Classes (%)	A (km²)	Area (%)
0 - 3	10033.62	22.93
3 – 12.5	19929.91	45.55
12.5 - 25	8452.62	19.32
> 25	5334.35	12.20
Total	43750.00	100.00

The lithological map of the Wadi Cheliff Basin, northwestern Algeria, illustrates its geological structure, surrounded by the Mediterranean Sea in the north (see Table 4). The legend demonstrates varied formations: alluvial and tuffaceous deposits (*A*), Cretaceous Inferieur continental (*ci*), Middle Cretaceous (*cm*), Upper cretaceous marine (*cs*), and recent dunes (*D*), among others, varying from Devonian (*F*) to Quaternary (*qv*). Northern sections close to Algiers consist of alluvial deposits (*A*) and Lower cretaceous (*ci*), which are sedimentary influence (Figure 6). Middle sections along Wadi Cheliff consist of Middle Cretaceous (*cm*) and Upper cretaceous marine (*cs*), which are marine and continental transitions. Southern sections consist of Middle Eocene marine (*em*) and Lower marine Miocene (*mi*), with Quaternary alluvial deposits (*qa*) and recent dunes (*D*) prevailing in the east.

Table 4. Lithology of the wadi Cheliff basin.

No.	Abbrev.	Lithological unit	Area (km²)	(%)
1	*A*	Current alluvium	43.34	0.10
2	*alfa*	Andesites and associated tuffs	17.13	0.04
3	*ci*	Lower cretaceous	4119.64	9.42
4	*cic*	Lower continental Cretaceous	1081.51	2.47

 doi:10.20944/preprints202602.1876.v1

5	*cj*	Unseparated cretaceous and Jurassic	19.25	0.04
6	*cm*	Middle Cretaceous	1757.51	4.02
7	*cn*	Cenomanian	433.63	0.99
8	*cs*	Upper cretaceous marine	3563.40	8.14
9	*ct*	Turonian	4088.13	9.34
10	*D*	Recent dunes	37.02	0.08
11	*d'*	Devonian	0.22	0.00
12	*ec*	Middle and lower continental Eocene	3.02	0.01
13	*ei*	Lower Eocene marine	992.67	2.27
14	*em*	Middle Eocene marine	1075.22	2.46
15	*gama*	Pegmatites	0.36	0.00
16	*j*	Jurassic	2.47	0.01
17	*ji*	Lower Jurassic marine	183.72	0.42
18	*jm*	Middle Jurassic	940.13	2.15
19	*jms*	Upper and middle Jurassic marine	7.28	0.02
20	*js*	Upper Jurassic	3949.99	9.03
21	*mc*	Antepontian continental Miocene	14.75	0.03
22	*mi*	Lower marine Miocene	2825.81	6.46
23	*mm*	Upper marine Miocene	2734.89	6.25
24	*mp*	Pontian	2235.25	5.11
25	*ms*	Terminal marine and lagoon Miocene	607.01	1.39
26	*o*	Marine Oligocene	1400.79	3.20
27	*oa*	Continental Aquitanian	47.86	0.11
28	*p*	Marine Pliocene	547.40	1.25
29	*pc*	Continental Pliocene	4234.46	9.68
30	*pV*	continental Pliocene and Villafranca not separated	339.65	0.78
31	*qc*	Calabrian	200.66	0.46
32	*qt*	Continental quaternary	5482.01	12.53
33	*Qv*	Villafranchian	489.10	1.12
34	*ro*	Rhyolites, dellenites, dacites and associated tuffs	5.37	0.01
35	*rt*	Premo Triassic	57.68	0.13
36	*t*	Marine or lagoon Triassic	211.66	0.48
Total			**43.750.00**	100,00

 doi:10.20944/preprints202602.1876.v1

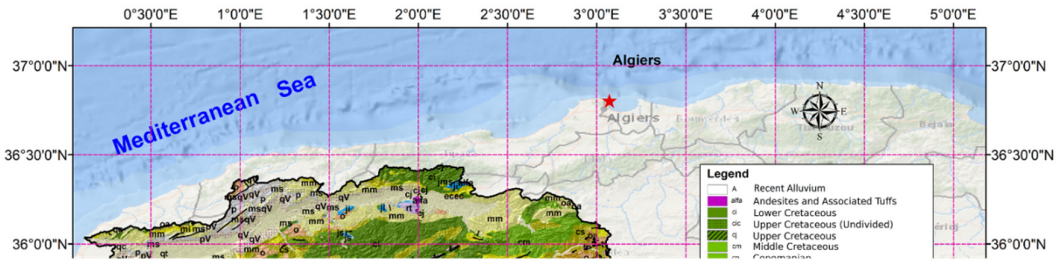

Figure 6. Lithological map of the study area.

3.1. Rainfall Erosivity Factor (R)

The mean annual rainfall erosivity factor (R) map of the Wadi Cheliff Basin (Figure 7) presents the rainfall erosivity (R) in MJ mm ha^{-1} h^{-1} y^{-1}, a key parameter for rill and sheet erosion and thus for the processes of soil erosion [65]. It is a representation of the high potential of soil loss under long-duration high-intensity rainfall. The northern part of the basin, nearer to the Mediterranean Sea, contains the highest R values (800–977), while in the south and southeastern parts there are smaller R values (191–300) and thus an implication of lower intensity of precipitation (Figure 8). It represents the impact of climatic and geographical parameters on erosivity. The map was generated using the inverse distance weighting interpolation technique from the observations of a network of rainfall gauging stations [65]. These spatial rain erosivity patterns are critical information for soil conservation and erosion control planning and sustainable land management planning in the Wadi Cheliff Basin.

 doi:10.20944/preprints202602.1876.v1

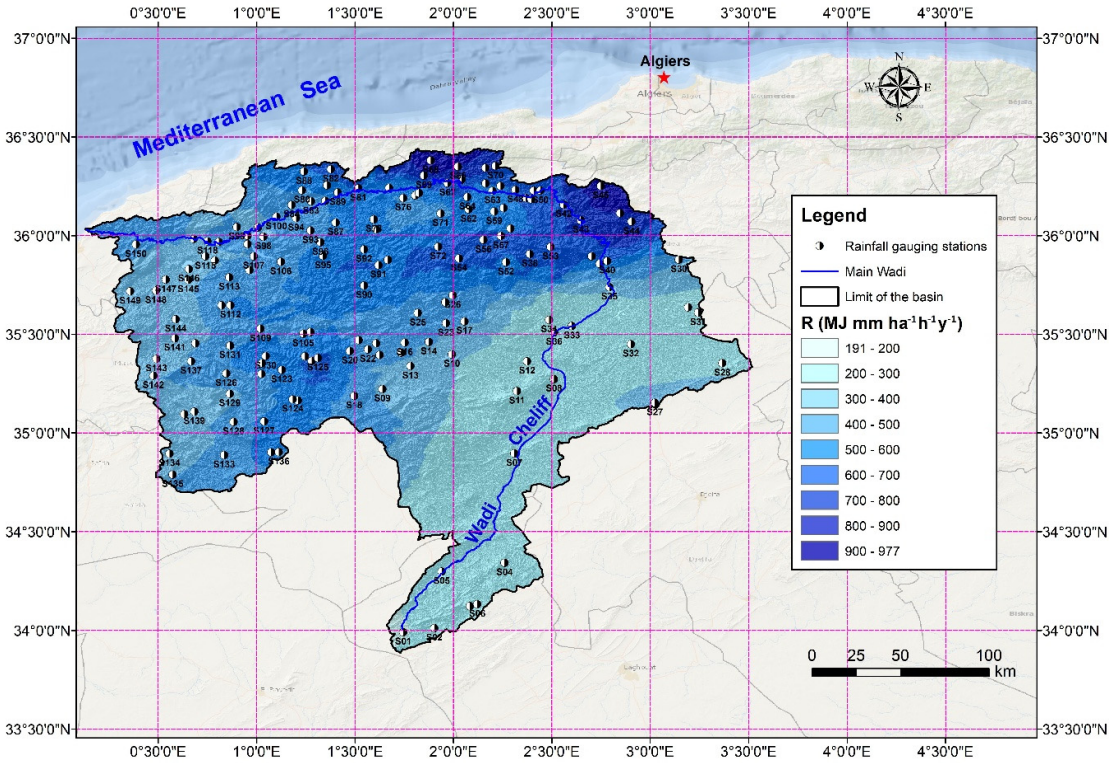

Figure 7. Spatial distribution of the mean annual rainfall erosivity factor (R) (1970-2018).

The map displays the rainfall distribution annually over the Wadi Cheliff basin in Algeria between 1970 and 2018 with values from 160 to 655 mm. The basin from the Mediterranean Sea close to Algiers in the north to the highlands in the south has an evident gradient of precipitation. The northern areas, especially around Algiers, have the highest precipitation, ranging from 500 to 655 mm, represented by darker blue colors, due to the Mediterranean climate effect (Figure 8). The southern and central regions of the basin, as well as parts along the main Wadi Cheliff, have lower precipitation, from 160 to 300 mm, represented by lighter colors, because of the semi-arid conditions further inland. The map also indicates rainfall measurement stations, offering data points for this long-term study, with the basin limits and principal wadi clearly defined for reference.

Spatial distribution of the highest daily rainfall (D, in mm) between 1970 to 2018 over the Wadi Cheliff basin is represented on the Figure 9. The basin is in northern Algeria and is bounded by the Mediterranean Sea to the north; the principal Wadi Cheliff traverses the area [66]. Rainfall intensity is quite variable across the basin. The northeast and north, the regions closer to the coast and the city of Algiers, present the highest values (50–54 mm), reflecting the greatest maritime influence. Rainfall declines towards the interior, with moderate values (35–45 mm) in the central and southwest regions (Figure 9). The southern and southeastern regions have the lowest values (19–30 mm), a reflection of more semi-arid climate characteristic of the interior. The spatial variation in rainfall distribution is due to topographical variation and proximity to the coast, which affects the water resource planning and erosion susceptibility of the basin [19]. It is vital for soil conservation planning and flood hazard forecasting in the Wadi Cheliff basin to comprehend these patterns spatially.

 doi:10.20944/preprints202602.1876.v1

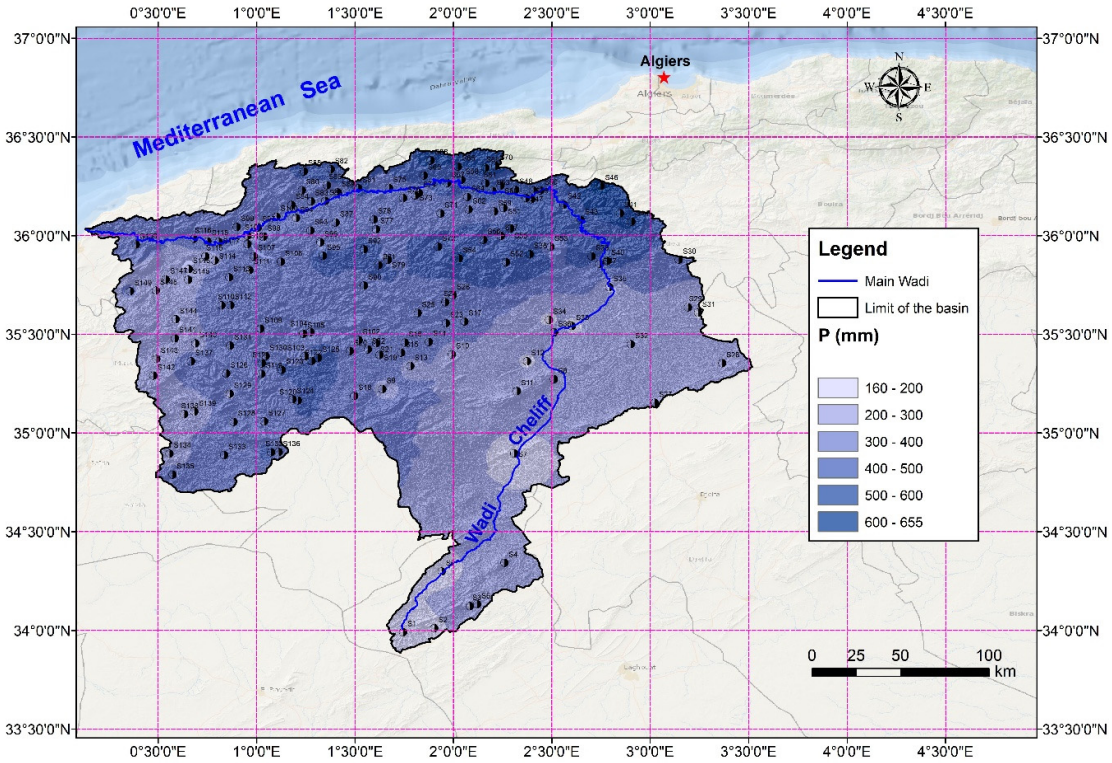

Figure 8. Spatial distribution of rainfall in the study area (1970-2018).

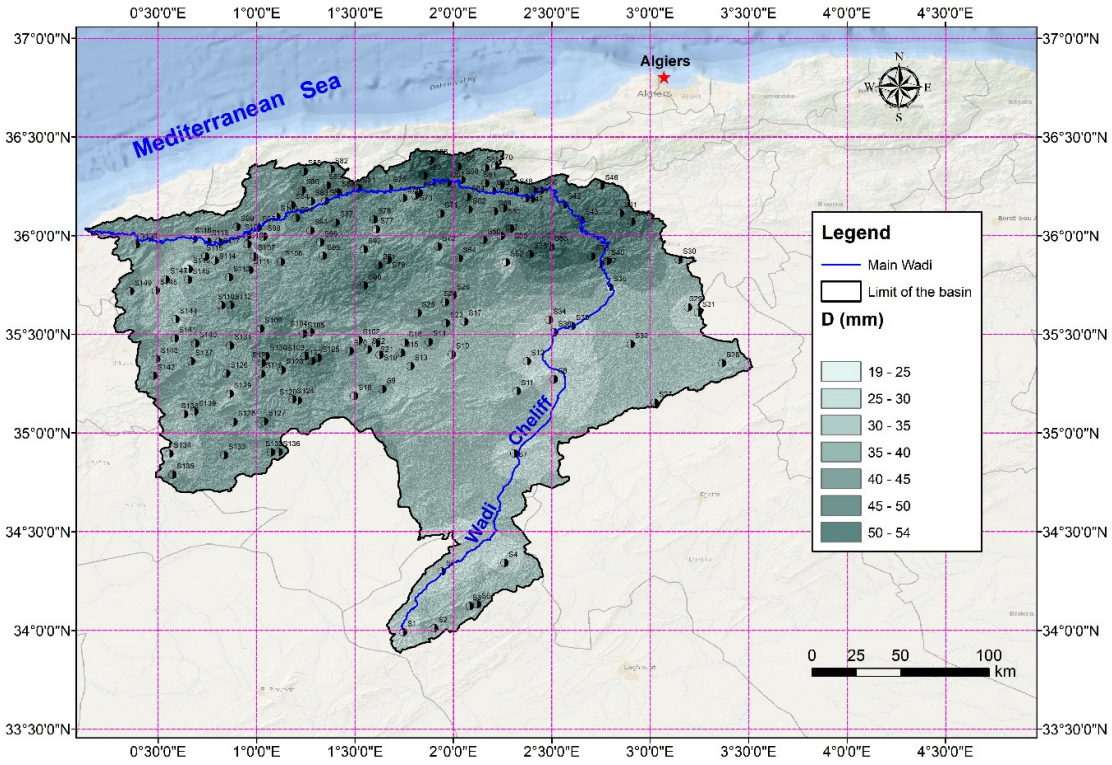

Figure 9. Spatial distribution of annual maximum daily rainfall in the study area (1970-2018).

 doi:10.20944/preprints202602.1876.v1

3.2. Soil Erodibility Factor (K)

Figure 10 shows the spatial distribution of the soil erodibility factor (K) within the Wadi Cheliff basin, Algeria. The K-factor in units of $t \cdot h \cdot MJ^{-1} \cdot mm^{-1}$ represents the susceptibility of soil to rain and runoff erosion [43]. The larger the value of K, the more sensitive the soil is, and the less sensitive the soil is to the smaller value. The map employed a color gradient where dark shades denote more erodible areas (K = 0.022), and light shades denote the less erodible areas (K = 0.01). The basin's main river, Wadi Cheliff, is represented by blue to depict the hydrological network and susceptible areas of erosion. The basin's edge is also depicted. The K-factor values are sourced from the Harmonized World Soil Database (HWSD v1.2), which is a global database, providing valuable data for erosion modeling, watershed planning, and soil conservation planning to reduce land degradation in the region.

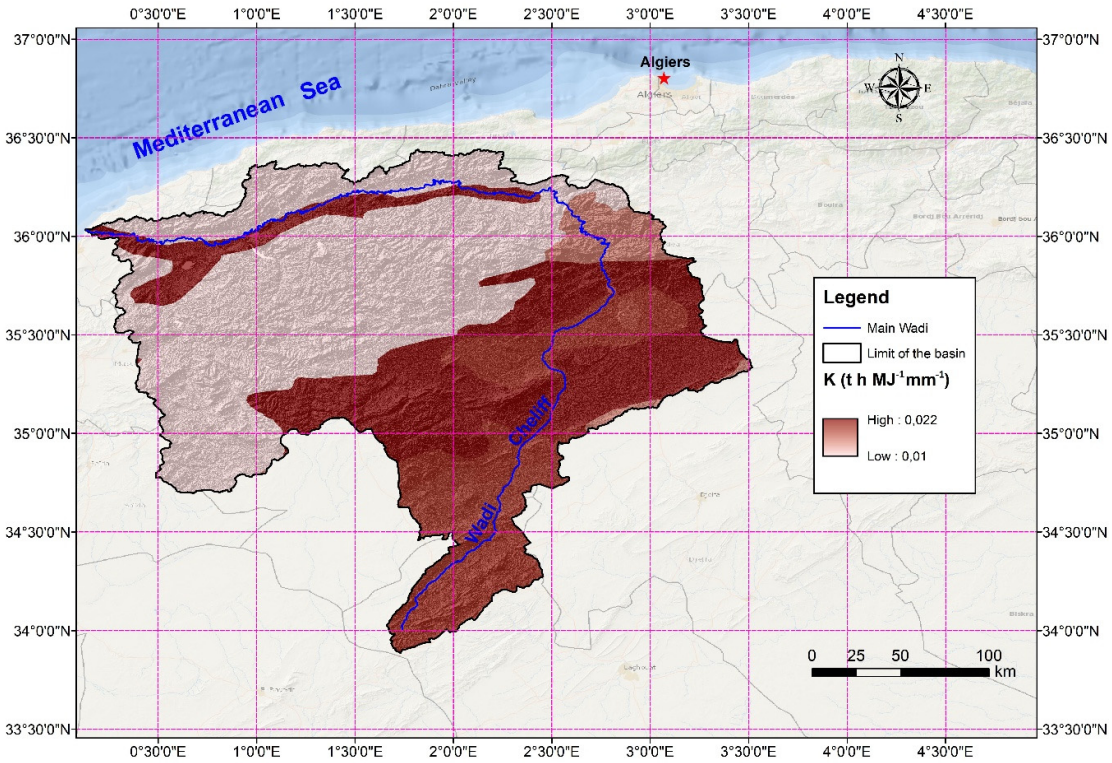

Figure 10. Spatial distribution of the K-Factor in the Wadi Cheliff basin.

3.3. Topographic Factor (LS)

Figure 11 illustrates Algeria's Wadi Cheliff basin LS factor of the RUSLE [44] as an average calculation of the combined effect of slope steepness (S) and slope length (L) on rain and runoff soil erosion [67]. The map classifies LS values from Algeria's Mediterranean coast to southern highlands into a color gradient. Greater LS values of 29.4783 and greater and darker tones are found in the mid and south regions of the basin, where greater slope angles and longer lengths of path of runoff increase erosion potential. The northern coastal region surrounding Algiers has less LS values, about 0 and light colors, which indicate flat regions with less erosion potential. The boundary of the basin and the Wadi Cheliff are clearly defined, and this offers a geographical template. Spatial distribution determines sheet and rill erosion areas that are susceptible, and this can be useful for targeted interventions to conserve soil.

 doi:10.20944/preprints202602.1876.v1

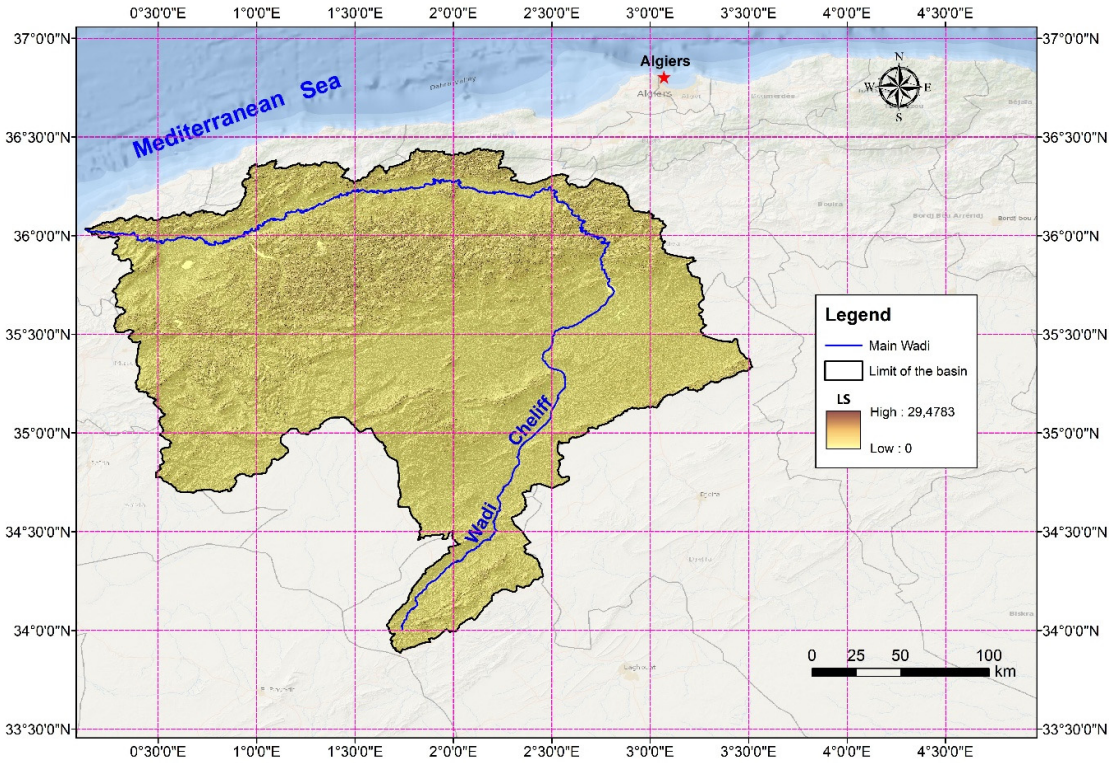

Figure 11. Spatial distribution of the LS factor in the Wadi Cheliff basin.

3.4. Crop Management Factor (C)

Figure 12 shows the C factor (October 2017) of the RUSLE for the Wadi Cheliff basin in Algeria, which represents the influence of vegetation cover and land use on soil erosion [68]. The basin, extending from the Mediterranean Sea north of Algiers to the south, has C factor values ranging from 0.047455 to 1.70722. Areas with greater C values (nearer to 1.70722), shown in darker shades, are predominantly located in the middle and southern regions, indicating sparse vegetation or improper land use, hence these areas are highly susceptible to erosion. Conversely, low C values (tending towards 0.047455), represented in the light shades, are found in the north regions along the coastline, exhibiting more vegetation cover or more protective management practices against erosion. The main Wadi Cheliff and basin limits are outlined, providing clear geographical reference to the assessment of erosion risk.

Figure 13 indicates Algeria's Wadi Cheliff basin C factor of the RUSLE as of May 2018, highlighting land use and vegetation cover effects on soil erosion [68]. The basin is from the Mediterranean Sea north of Algiers south to the southern highlands. The C factor values range from 0.0328544 to 1.99076, and the corresponding color ranges from green to red. The areas with higher C values (closer to 1.99076), in red, are in the south and middle, indicating thin vegetation or poor management, and therefore these areas are most prone to erosion. In contrast, regions with smaller C values (tending towards 0.0328544), colored green, occur largely in northern coastal areas, meaning denser vegetation or enhanced land use with better resistance to erosion. The main Wadi Cheliff and basin margins are clearly marked for identification.

 doi:10.20944/preprints202602.1876.v1

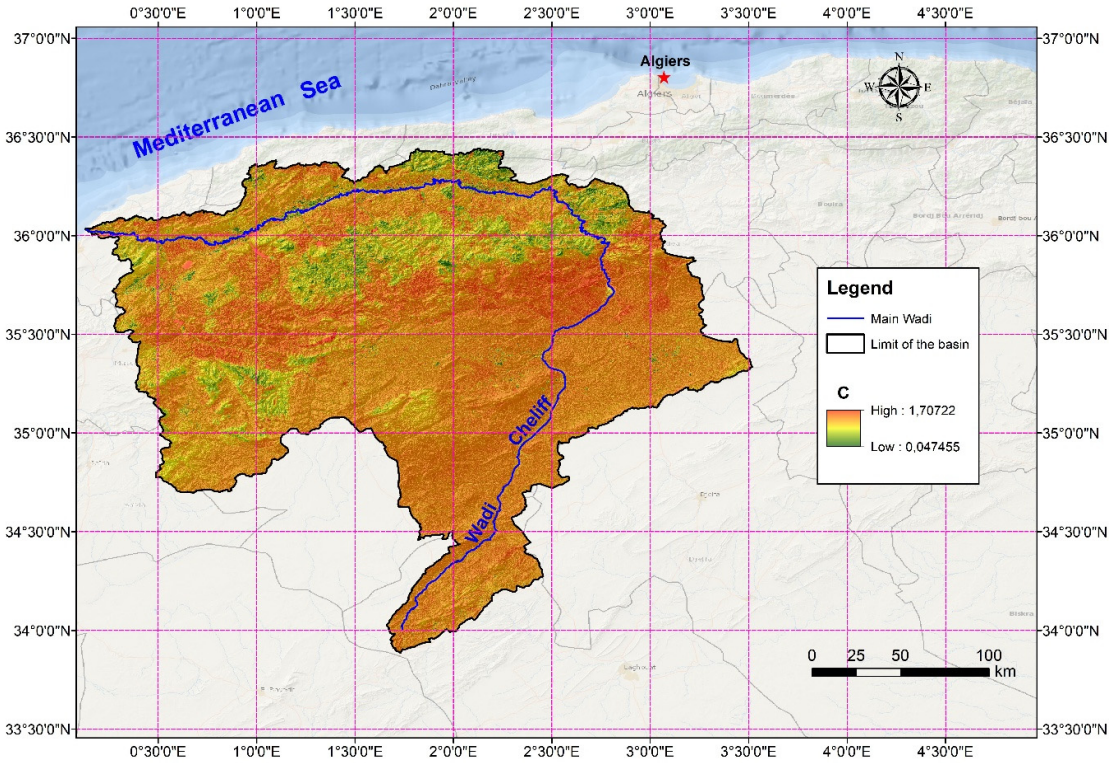

Figure 12. Spatial distribution of the C factor for October 2017.

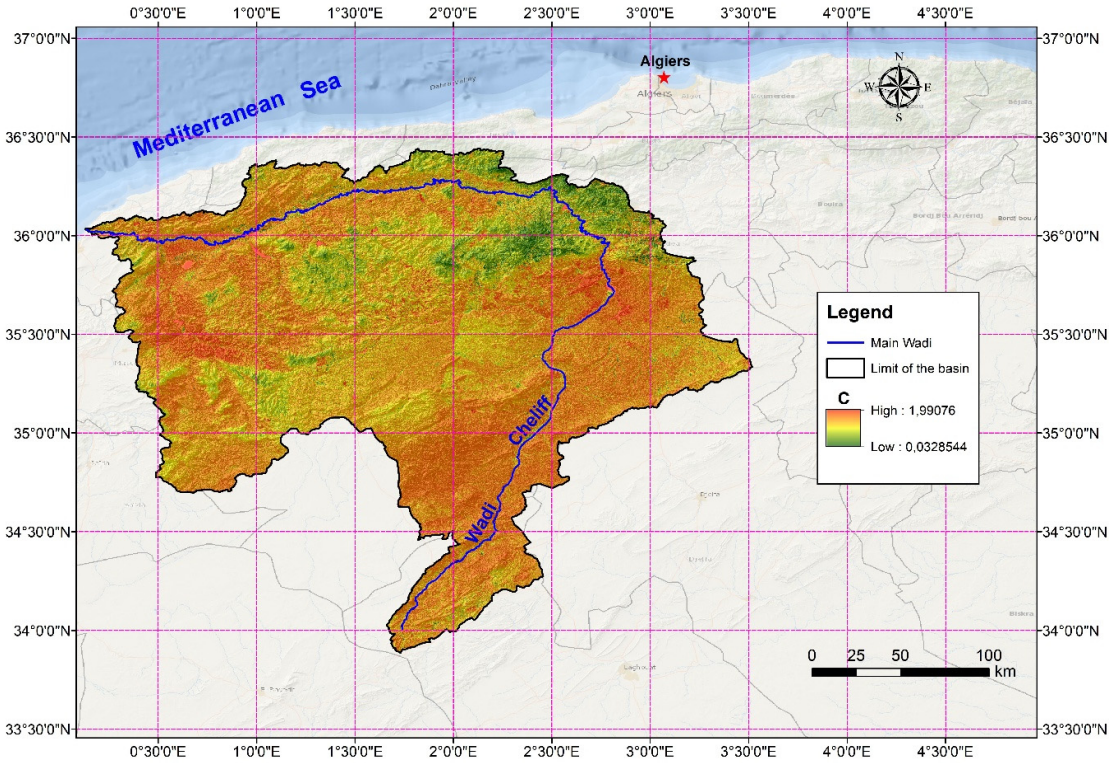

Figure 13. Spatial distribution of the C factor for May 2018.

 doi:10.20944/preprints202602.1876.v1

3.5. Conservation Support Practice Factor (P)

Figure 14 shows the spatial variability of the conservation support practice factor (P) in the wadi Cheliff basin. The value varies from 0 for good conservation practices to 1 for poor conservation practices. For our case study, the area has an P factor in the range of 0.6–0.95, with an average value of 0.63.

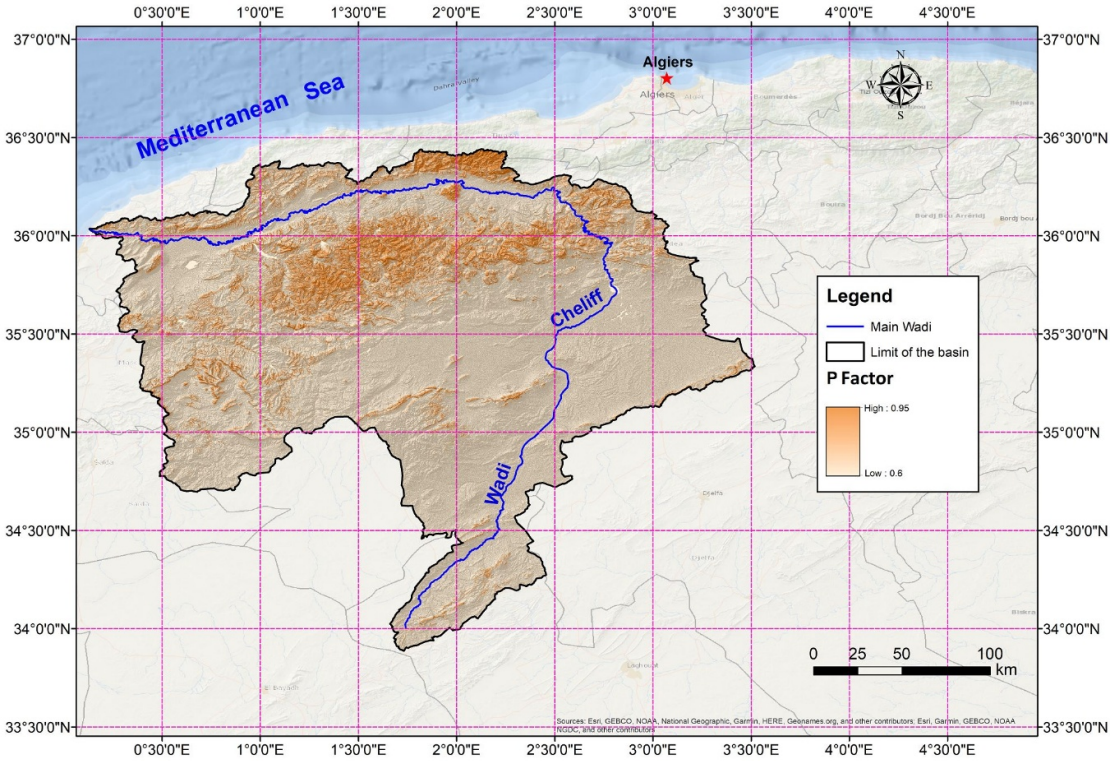

Figure 14. Spatial distribution of the P factor in the Wadi Cheliff basin.

3.6. Evaluation of Soil Erosion in the Wadi Cheliff Basin Using the RUSLE Model

Figure 15 shows the soil erosion rates (A, t ha¹ year¹) in the Wadi Cheliff basin based on implemented RUSLE model (October 2017). The rates are strongly heterogeneous because of topography, land use, and precipitation regimes. The northern and central parts of the basin with steep slopes and sparse vegetation cover possess high rates of erosion (20–50 t ha^{-1} a^{-1}), and a few localized points possess even more higher rates higher than 50 t ha^{-1} a^{-1}. They are the most prone areas due to the high rainfall intensity events, sparse vegetation cover, and steep slope. By comparison, the south and southwest sections have low to moderate levels of erosion (0–10 t ha¹ year¹), primarily from less steep slope angles and enhanced plant cover. Risk of erosion lessens as land is flattened and as vegetation is stabilizing. The east areas of the basin have moderate levels of erosion (10–20 t ha-¹ year¹), indicating a combination of various slope grades and moderate cover by vegetation. The map highlights the importance of soil conservation measures, especially in susceptible northern and central areas, to mitigate soil degradation and promote sustainable land use practices. Spatial patterns are known to give high priority to erosion control measures and provide effective soil management practices.

 doi:10.20944/preprints202602.1876.v1

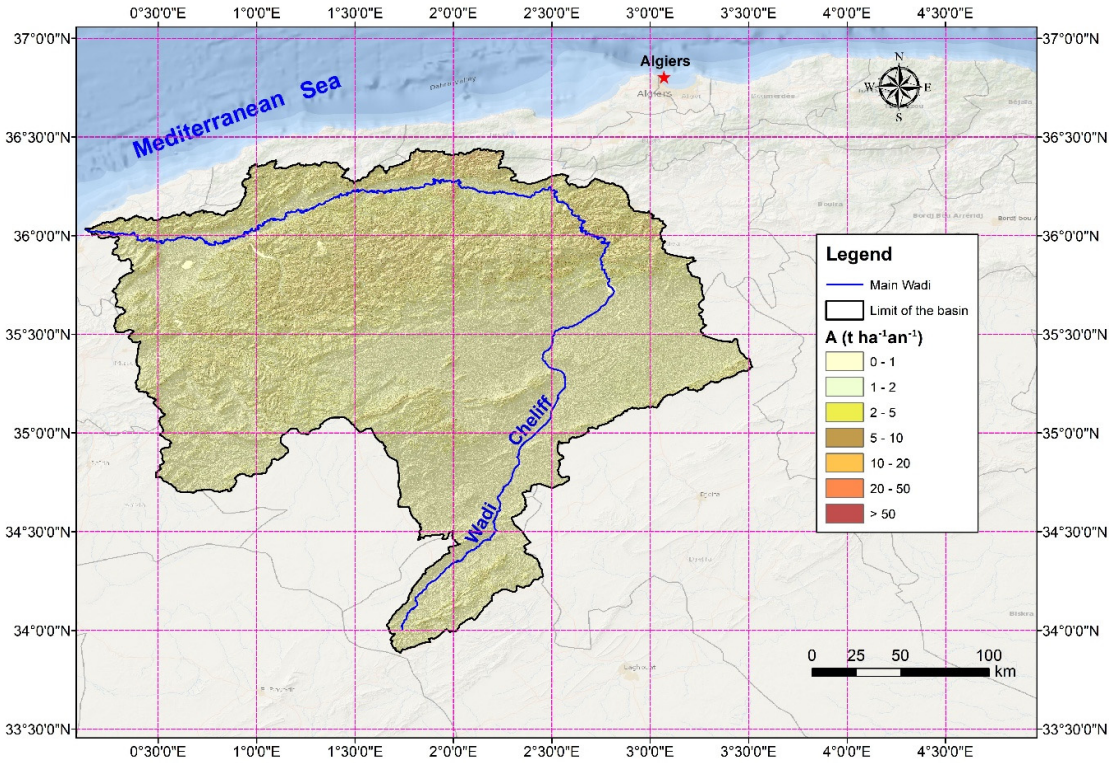

Figure 15. Spatial distribution of average soil erosion rates in the Wadi Cheliff basin (October 2017).

Figure 16 shows the distribution of the rates of soil erosion (A, t ha-^{1} a-^{1}) of the Wadi Cheliff basin in May 2018, which was estimated by means of the RUSLE model. It varies considerably as a function of rainfall, cover vegetation, and topography. North and north-central parts possess high intensities of erosion (20–50 t ha^{-1} a^{-1}), with foci reaching values close to 50 t ha^{-1} a^{-1}, primarily due to slopes and open vegetation. The south and south-west regions possess low erosion intensities (0–5 t ha^{-1} a^{-1}) due to levelled slopes and closed vegetation cover that restricts soil movement. The east segments possess moderate erosion rates (5–20 t ha^{-1} a^{-1}), which represent mixed topography and vegetation cover. This regional heterogeneity highlights the importance of implementing soil conservation practices in high-risk northern regions, such as afforestation and slope stabilization, and maintaining protective vegetative cover in low-risk regions for sustainable use.

 doi:10.20944/preprints202602.1876.v1

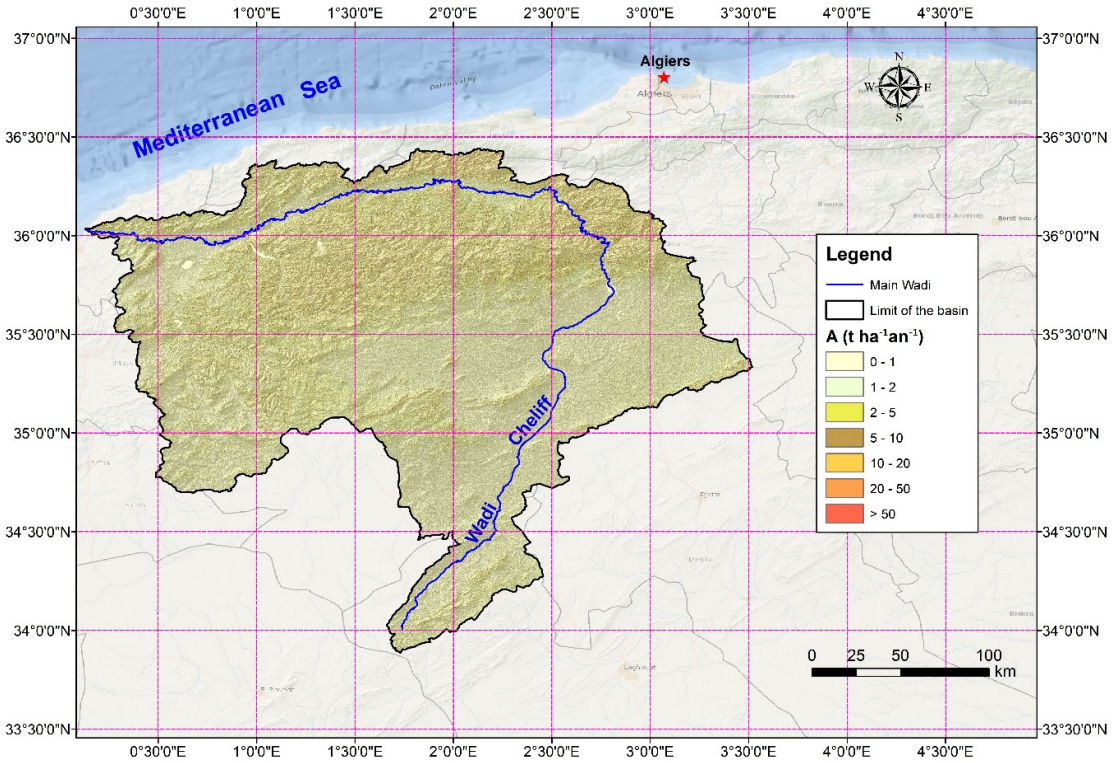

Figure 16. Spatial distribution average soil erosion rates in the Wadi Cheliff basin (May 2018).

Table 5 shows the spatial distribution of soil loss classes in the Wadi Cheliff Basin for 2017 and 2018. The majority of the basin area is under very low erosion risk (0–1 t ha^{-1} yr^{-1}), covering 90.73% in 2017 and increasing to 92.28% in 2018. Moderate to high erosion classes (2–50 t ha^{-1} yr^{-1}) occupy a small portion of the basin, with slight differences between the two years. Areas with extreme erosion (>50 t ha^{-1} yr^{-1}) remain very limited, representing only 0.02% in 2017 and 0.40% in 2018. Overall, these results indicate that most of the basin experiences low erosion rates, with localized hotspots of higher soil loss, and that the mean soil loss decreased from 0.70 t ha^{-1} yr^{-1} in 2017 to 0.57 t ha^{-1} yr^{-1} in 2018, suggesting a slight reduction in overall erosion intensity, likely due to changes in rainfall or improved land cover.

Table 5. Area under different categories of soil erosion in Wadi Cheliff basin using RUSLE model.

Area 2017 (A mean = 0.70 t ha-1 yr-1)		
Erosion classes (t ha-1 yr-1)	Area (km²)	Area (%)
0 – 1	39684.72	90.73
1 – 2	1277.05	2.9
2 – 5	1460.39	3.34
5 – 10	727.9	1.66
10 – 20	419.3	0.96
20 – 50	170.98	0.39
>50	9.66	0.02
Total	43,750.00	100.00
Area 2018 (A mean = 0.57 t ha-1 yr-1)		

 doi:10.20944/preprints202602.1876.v1

Erosion classes (t ha-1 yr-1)	Area (km²)	Area (%)
0 – 1	40374.2	92.28
1 – 2	183.45	0.42
2 – 5	1488.3	3.40
5 – 10	788.61	1.80
10 – 20	479.8	1.10
20 – 50	261.15	0.60
>50	174.5	0.40
Total	43,750.00	100.00

Table 6 summarizes the descriptive statistics of the RUSLE factors, highlighting their magnitude and spatial variability across the study area. The rainfall erosivity factor (R) exhibits a wide range of values (191.35–901.54), with a mean of 416.48 and a coefficient of variation (CV) of 0.36. This moderate variability reflects pronounced spatial differences in rainfall aggressiveness, which is a key driver of soil erosion in the basin. The soil erodibility factor (K) shows a narrow range (0.014–0.023) and a low CV (0.205), indicating relatively homogeneous soil properties at the basin scale. This suggests that, compared to other factors, soil texture and structure contribute less to spatial contrasts in erosion risk. In contrast, the topographic factor (LS) displays very high variability, with values ranging from 0 to 29.48 and a CV of 3.08. This strong heterogeneity highlights the dominant role of slope length and steepness in controlling erosion processes, especially in areas with rugged terrain.The cover-management factor (C) for 2017 and 2018 shows moderate mean values (0.76 and 0.65, respectively) and relatively low CVs (0.12–0.21). These results indicate limited interannual variability in vegetation cover, although the slightly lower mean in 2018 suggests an improvement in protective land cover conditions compared to 2017. The support practice factor (P) has a mean value of 0.63 and a low CV (0.11), implying fairly uniform land management practices across the basin, with limited spatial differentiation in conservation measures. Finally, the computed soil loss (A) exhibits very high variability in both 2017 and 2018, with CVs of 3.91 and 3.70, respectively. Maximum soil loss values (224.00 t·ha^{-1}·yr^{-1} in 2017 and 204.10 t·ha^{-1}·yr^{-1} in 2018) indicates that severe erosion is concentrated in localized hotspots rather than being widespread. The lower mean and maximum soil loss in 2018 further suggest a slight reduction in erosion intensity, likely linked to improved vegetation cover or interannual rainfall differences. Overall, the results emphasize that topography (LS) and rainfall erosivity (R) are the main sources of spatial variability in soil erosion, while soil properties, land cover, and conservation practices are comparatively more homogeneous at the basin scale.

Table 6. Summary statistics for the different factors of the RUSLE model.

Values	R	K	LS	C 2017	C 2018	P	A 2017	A 2018
Minimum	191.35	0.014	0	0.05	0.03	0.60	0.00	0.0
Maximum	901.54	0.023	29.48	1.71	1.99	0.95	224.00	204.10
Mean	416.48	0.018	0.18	0.76	0.65	0.63	0.70	0.57
St. deviation	148.50	0.004	0.56	0.09	0.13	0.07	2.74	2.11
Coefficient of variation (CV)	0.36	0.205	3.08	0.12	0.21	0.11	3.91	3.70

4. Discussion

Use of the RUSLE across the Wadi Cheliff Basin indicates a multi-dimensional interaction of climatic, topographic, and land-use controls on soil erosion, with important implications for sustainable land management. Soil loss spatial heterogeneity (A), spanning between October 2017 to May 2018 with ranges 0–50 t ha^{-1} a^{-1}, represents combined effect of rainfall erosivity (R), erodibility

 doi:10.20944/preprints202602.1876.v1

(K) of the soil, topography (LS) and cover and management factor (C). The results substantiate with the tendency in erosion susceptibility patterns across the Mediterranean semi-arid catchment regions, with where there has increased gradient aggravating environment with rising dangers on soil deterioration [9].

The rainfall erosivity factor (R) value map 191–977 MJ mm ha^{-1} h^{-1} y^{-1} from 1970 to 2018 reflects the contribution made by precipitation intensity to erosion. Consequently, the higher rainfall erosivity in the northern part of the basin accounts for the increased soil loss rates observed there (20–50 t ha^{-1} a^{-1}), as heavy rain events could better detach and transport soil particles [20]. Studies on the Cheliff region, including Saoud and Meddi (2022) [69] have similarly found that one gets higher erosivity in the north due to coastal proximity and agreeing with our finding. On the other hand, lower R values (191–300) in the south and southeast, and low rainfalls (160–300 mm), are indicative of a semi-arid condition with less erosive potential, leading to minimal soil loss (0–10 t ha^{-1} a^{-1}). Rainfall erosivity higher than 1000 MJ mm ha^{-1} h^{-1} yr^{-1} was detected in Italy, southern France, Croatia, Slovenia, Pyrenees, Andalusia, Galicia (Spain) [70]. This pattern highlights the role of orographic enhancement together with maritime influence, both of which are defining characteristics of coastal Mediterranean climatic regimes.

Soil erodibility (K) with 0.01–0.022 t h MJ^{-1} mm^{-1} values indicates the spatial distribution of erosion susceptibility further. Higher numbers of K values with higher values in the north and center (0.022) indicate finer textures or lower organic content proportions, which are more prone to detachment [55]. Bensekhria and Bouhata (2022) [71] also revealed the same soil properties in the Cheliff Basin where increased K values correlated with increased erosion hazard in the respective areas. Alternatively, low K values (0.01) in the south indicate challenging soils that do not erode despite topographic difficulties. The trend is in accordance with studies for semi-arid areas [72].

Topographic factor (LS) with its highest value of 29.4783 in the middle and southern highlands ranks slope steepness and length as the most dominant factors for increasing erosion. The steeper slopes increase the speed of runoff, and hence soil loss, especially where high values of LS occur [9]. Hamadouche et al. (2020) [73] reported that the topography of mid-Cheliff Basin strengthens the erosion on high slopes, a finding which confirms our high values for LS and corresponding rates of soil loss (20–50 t ha-^{1} yr-1). The minimum values of LS close to 0 for northern coastal plains confirm low erosion for flat terrain, as observed e.g. in the lowlands of Southern Italy [4].

The cover-management index (C) values of October 2017 (0.047455–1.70722) and May 2018 (0.0328544–1.99076) reflect vegetation seasonality and spatiality and land-use patterns. Values of C (near 1.99076) for the central and southern parts indicate poor management or low vegetation, which has high erosion rates. These results are consistent with findings from arid landscapes in Pakistan, as reported by Rashid et al. (2025) [74].

Zeghmar et al. (2022) [75] also showed that low vegetation cover in southern Cheliff Basin increases the susceptibility of erosion, thereby validating our results. The lower C values (most close to 0.0328544) for north coastal regions indicate higher plant cover or improved methodology, lowering erosion to 0–10 t ha^{-1} a^{-1}. Seasonal variation between October and May indicates that recovery vegetation following rains during winter improves soil cover in the north.

Excessive erosion in the middle and north basin lowers the soil fertility and increases sediment load in Wadi Cheliff [55]. Cherif et al. (2023) [76] emphasized very strongly that all these sediment dynamics of the Cheliff region complicate watershed management, again in agreement with our recommendation of specialized conservation practices like terracing and afforestation. Lower erosion rates of the southern parts mean that there is a scope for sustainable agriculture if water could be managed [9]. The spatial patterns revealed herein provide some insight into how such initiatives must be ranked in the Wadi Cheliff Basin. At the temporal scale, very low erosion risk (0–1 t ha^{-1} yr^{-1}) dominates the basin, accounting for 90.73% of the area in 2017 and increasing to 92.28% in 2018. Overall, the Wadi Cheliff basin is characterized by generally low soil erosion rates, with higher soil loss confined to limited, localized hotspots. Consistent with this pattern, the mean annual soil loss declined from 0.70 t ha^{-1} yr^{-1} in 2017 to 0.57 t ha^{-1} yr^{-1} in 2018, indicating a slight improvement in

 doi:10.20944/preprints202602.1876.v1

erosion conditions over time. Previous studies conducted by Zerouali et al. (2025) [77] and Toumi and Meddi (2026) [78] identified a larger proportion of the Cheliff basin as moderately eroded (31% of basin was affected) while soil loss varies from 0 to 165 t/ha/yr, with an average of 18.3 t/ha/yr. Differences between the presented results and those reported by Zerouali et al. (2025) [77] and Toumi and Meddi (2026) [78] can be explained by variations in methodology, input datasets, spatial resolution, and temporal scales. However, the present study which is based on year-specific climatic data and spatially explicit modeling – showed that very low erosion risk dominates most of the basin, with higher erosion limited to localized hotspots. In this context, the present study highlights the need for consistent and spatially representative long-term field measurements and data to validate model outputs and better reconcile differences between erosion assessments.

Finding similar results at regional and national scales is challenging; however, certain patterns can be identified. For example, in Mediterranean and arid environments such as watershed in Greece, estimated annual erosion rates were in the range of 0–0.6 t/ha/yr [79] which is less in compare to the average annual loss in the Wadi Chaliff basin; Menghis et al. (2025) [80] identified in Eritrea the low erosion in the most of the investigated watershed (68.19%); on the contrary, Fadl et al. (2025) [81] revealed that 41% of the Mitidja Plain (Algeria) is at severe erosion risk, with an average soil loss of 88.72 t ha^{-1} yr^{-1}. Similarly, the annual rate of soil erosion in the Lattakia (Syria) was 81.1 t ha^{-1} $year^{-1}$ [82]. Nieto et al. (2024) [83] detected high vulnerable zones in the northwestern part of Spain that showed severe erosion rates exceeding 50 t/ha/year (>5 mm/year), with the most extreme zones reaching up to 200 t/ha/year (>200 mm/year).

These impacts are of great importance in water resource management and soil erosion prevention, as they directly affect watershed hydrology, sediment transport, agricultural productivity, and the long-term sustainability of land use. Understanding spatial and temporal patterns of soil erosion also supports the design of effective soil conservation measures, reduces downstream sedimentation in reservoirs and rivers, and mitigates the risk of floods and land degradation.

5. Conclusions

The study aimed to quantify and model the water erosion in the Wadi Cheliff basin in order to address the need for spatial and temporal understanding of soil erosion dynamics. In the context of global change, understanding erosion patterns in vulnerable Mediterranean basins is critically important for informing land management and policy development. In this regard, the RUSLE model has been widely applied to provide a robust foundation for the design and implementation of effective erosion control practices.

The RUSLE model revealed intensive spatial heterogeneity of soil loss, varying from 0–50 t ha^{-1} a^{-1} in the Wadi Cheliff Basin from October 2017 to May 2018. Northern regions close to the Mediterranean region revealed high erosion (20–50 t ha^{-1} a^{-1}) due to high rainfall erosivity (800–977 MJ mm ha^{-1} h^{-1} y^{-1}) and high slopes (LS up to 29.4783), whereas low erosion (0–10 t ha^{-1} a^{-1}) was revealed with low precipitation and less sloping. These trends were characterized by intensity of rainfall, soil erodibility (K: 0.01–0.022 t h MJ^{-1} mm^{-1}), and change in vegetation cover (C: 0.0328544–1.99076).

These findings demonstrate the critical significance of climatic and topographic gradients to regulate processes of erosion, being instrumental in supplying valuable knowledge to soil conservation in semi-arid regions. Increased erosion in the northern and central basin threatens the fertility of soil and increases sedimentation loads, compromising water resource management. Spatial erosion risk maps provide policymakers with an effective tool to identify priority areas for conservation and to optimize sustainable land-use planning. Future research must consider seasonal dynamics of vegetation change and their influence on the C-factor to further enhance erosion estimation, particularly in relation to the derived May to October transitions detected. With inclusion of observed rainfall and extension of the observation period to cover more years should reduce record gaps (0–30% missing data). The RUSLE-based field validation in highly risk-exposed localities would

 doi:10.20944/preprints202602.1876.v1

further add strength to conservation planning. The article demands that soil erosion in the Wadi Cheliff Basin be addressed to help buffer land degradation in the face of increasing environmental pressure.

As limitation of this study, the main points are: a) Digital Elevation Model (DEM) Quality, b) lack of National Soil Database in sense of detailed, spatially explicit soil maps with the required parameters (texture, organic matter, structure) and c) the lack of observed sediment data. There is a critical shortage of measured sediment yield data from watersheds or experimental plots to calibrate and validate RUSLE predictions. Validation will help refine these results and improve their reliability.

By integrating science-based modeling with operation management, this study can contribute towards the general objective of Mediterranean ecosystem conservation. Implementing effective erosion control is essential to sustain long-term agricultural productivity and environmental stability in the region.

Author Contributions: All authors contributed equally to the study's conception and design. conceptualization, M.A. and A.K.T.; methodology, M.A., and A.K.T.; software, M.A., and N.M.M.; formal analysis, M.A., N.M.M.; validation: M.A., P.C., P.N., N.E., N.M.M. and T.C.; investigation, M.A., and P.C and N.M.M..; data curation, M.A. and A.K.T.; writing—original draft preparation, M.A., P.C., P.N., N.E., N.M.M. and T.C., writing—review and editing, M.A., P.C., P.N., N.E., N.M.M. and T.C.; supervision, N.M.M. and T.C. All authors have read and agreed to the published version of the manuscript. All authors read and approved the final manuscript.

Funding: The authors declare that no funds, grants, or other support were received during the preparation of this manuscript.

Data Availability Statement: Not applicable.

Acknowledgments: The authors gratefully acknowledge the National Agency for Water Resources (ANRH) and the General Directorate of Scientific Research and Technological Development of Algeria (DGRSDT) for their support.

Conflicts of Interest: The authors declare that they have no known competing financial interests or personal relationships that could have appeared to influence the work reported in this paper.

References

1. Sulaeman, D.; Westhoff, T. *The causes and effects of soil erosion, and how to prevent it.* World Resources Institute: Washington, DC, United States, 2020.
2. Ahmad, N.S.B.N.; Mustafa, F.B.; Didams, G. A systematic review of soil erosion control practices on the agricultural land in Asia. *Int. Soil Water Conserv. Res.* **2020**, *8*(2), 103-115. https://doi.org/10.1016/j.iswcr.2020.04.001
3. Sharda, V.N.; Ojasvi, P.R. A revised soil erosion budget for India: role of reservoir sedimentation and land-use protection measures. *Earth Surf. Process. Landf.* **2016**, *41*(14), 2007-2023. https://doi.org/10.1002/esp.3965
4. Covelli, C.; Cimorelli, L.; Pagliuca, D.N.; Molino, B.; Pianese, D. Assessment of erosion in river basins: A distributed model to estimate the sediment production over watersheds by a 3-Dimensional LS Factor in RUSLE Model. *Hydrology* **2020**, *7*(1), 13. https://doi.org/10.3390/hydrology7010013
5. Djoukbala, O.; Hasbaia, M.; Benselama, O.; Hamouda, B.; Djerbouai, S.; Ferhati, A. Water Erosion and Sediment Transport in an Ungauged Semiarid Area: The Case of Hodna Basin in Algeria. In *Wadi Flash Floods. Natural Disaster Science and Mitigation Engineering: DPRI reports*. Sumi, T., Kantoush, S.A., Saber, M. Eds.; Springer: Singapore, 2022, pp. 439-454. https://doi.org/10.1007/978-981-16-2904-4_17
6. Borrelli, P.; Robinson, D.A.; Fleischer, L.R. et al. An assessment of the global impact of 21st century land use change on soil erosion. *Nat. Commun.* **2017**,8, 2013. https://doi.org/10.1038/s41467-017-02142-7
7. Kayet, N.; Pathak, K.; Chakrabarty, A.; Sahoo, S. Evaluation of soil loss estimation using the RUSLE model and SCS-CN method in hillslope mining areas. *Int. Soil Water Conserv. Res.* **2018**, *6*(1), 31-42. https://doi.org/10.1016/j.iswcr.2017.11.002

 doi:10.20944/preprints202602.1876.v1

8. Dinka, M.O. Quantification of soil erosion and sediment yield for ungauged catchment using the RUSLE model: Case study for Lake Basaka catchment in Ethiopia. *Lakes & Reserv*. **2020**, *25*(2), 183-195. https://doi.org/10.1111/lre.12312
9. Borrelli, P., Robinson, D. A., Panagos, P., Lugato, E., Yang, J. E., Alewell, C. et al. Land use and climate change impacts on global soil erosion by water (2015-2070). *Proc. Natl. Acad. Sci. U.S.A.* **2020**, *117*(36), 21994-22001. https://doi.org/10.1073/pnas.2001403117
10. Gholami, L.; Khaledi Darvishan, A.; Spalevic, V.; Cerdà, A.; Kavian, A. Effect of storm pattern on soil erosion in damaged rangeland; field rainfall simulation approach. *J. Mt. Sci.* **2021**, *18*, 706–715. https://doi.org/10.1007/s11629-019-5633-2
11. Fang, H.; Fan, Z. Assessment of Soil Erosion at Multiple Spatial Scales Following Land Use Changes in 1980–2017 in the Black Soil Region, (NE) China. *Int. J. Environ. Res. Public Health* **2020**, *17*, 7378. https://doi.org/10.3390/ijerph17207378
12. Eniyew, S.; Teshome, M.; Sisay, E.; Bezabih, T. Integrating RUSLE model with remote sensing and GIS for evaluation soil erosion in Telkwonz Watershed, Northwestern Ethiopia. *Remote Sens. Appl.: Soc. Environ.*, **2021**, *24*, 100623. https://doi.org/10.1016/j.rsase.2021.100623
13. Pal, S.C.; Chakrabortty, R.; Roy, P.; Chowdhuri, I.; Das, B.; Saha, A.; Shit, M. Changing climate and land use of 21st century influences soil erosion in India. *Gondwana Res.* **2021**, *94*, 164-185. https://doi.org/10.1016/j.gr.2021.02.021
14. Kaur, B.; Sur, K.; Verma, V.K.; Pateriya, B. Implications of watershed management programs for sustainable development in rural scenario—a case study from foothills of Punjab state, India. *Water Conserv. Sci. Eng.* **2022**, **7**, 647–655. https://doi.org/10.1007/s41101-022-00170-z
15. Medjani, F.; Derradji, T.; Zahi, F.; Djidel, M.; Labar, S.; Bouchagoura, L. Assessment of soil erosion by Universal Soil Loss Equation model based on Geographic Information System data: a case study of the Mafragh watershed, north-eastern Algeria. *Sci. African*, **2023**, *21*, e01782. https://doi.org/10.1016/j.sciaf.2023.e01782
16. Maltsev, K.; Yermolaev, O. Assessment of soil loss by water erosion in small river basins in Russia. *Catena*, **2020**, *195*, 104726. https://doi.org/10.1016/j.catena.2020.104726
17. Abdelwahab, O.M.M.; Ricci, G.F.; De Girolamo, A.M.; Gentile, F. Modelling soil erosion in a Mediterranean watershed: Comparison between SWAT and AnnAGNPS models. *Environ. Res.* **2018**, *166*, 363-376. https://doi.org/10.1016/j.envres.2018.06.029
18. Singh, M.C.; Sur, K.; Al-Ansari, N.; Arya, P.K.; Verma, V.K.; Malik, A. GIS integrated RUSLE model-based soil loss estimation and watershed prioritization for land and water conservation aspects. *Front. Environ. Sci.* **2023**, *11*, 1136243. doi: 10.3389/fenvs.2023.1136243
19. Wischmeier, W.H.; Smith, D.D. *Predicting Rainfall Erosion Losses: A Guide to Conservation Planning*; Agriculture Handbook No. 537; U.S. Department of Agriculture: Washington, DC, USA, 1978.
20. Renard, K.G.; Foster, G.R.; Weesies, G.A.; McCool, D.K.; Yoder, D.C. *Predicting Soil Erosion by Water: A Guide to Conservation Planning with the Revised Universal Soil Loss Equation (RUSLE)*; Agriculture Handbook No. 703; U.S. Department of Agriculture, Agricultural Research Service: Washington, DC, USA, 1997.
21. Kumar, P.S.; Praveen, T.V.; Prasad, M.A. Simulation of sediment yield over un-gauged stations using MUSLE and fuzzy model. *Aquatic Procedia* **2015**, *4*, 1291–1298. https://doi.org/10.1016/j.aqpro.2015.02.168
22. Grum, B.; Woldearegay, K.; Hessel, R.; Baartman, J.E.; Abdulkadir, M.; Yazew, E.; Geissen, V. Assessing the effect of water harvesting techniques on event-based hydrological responses and sediment yield at a catchment scale in northern Ethiopia using the Limburg Soil Erosion Model (LISEM). *Catena* **2017**, *159*, 20–34. https://doi.org/10.1016/j.catena.2017.07.018
23. Pieri, L.; Bittelli, M.; Wu, J.Q.; Dun, S.; Flanagan, D.C.; Pisa, P.R.; Salvatorelli, F. Using the Water Erosion Prediction Project (WEPP) model to simulate field-observed runoff and erosion in the Apennines mountain range, Italy. *J. Hydro.* **2007**, *336*(1-2), 84–97.
24. Vigiak, O.; Malagó, A.; Bouraoui, F.; Vanmaercke, M.; Poesen, J. Adapting SWAT hillslope erosion model to predict sediment concentrations and yields in large basins. Sci. Total Environ. 2015, 538, 855–875. https://doi.org/10.1016/j.scitotenv.2015.08.095

 doi:10.20944/preprints202602.1876.v1

25. Morgan, R.P.C.; Morgan, D.D.V.; Finney, H.J. A predictive model for the assessment of soil erosion risk. *J. Agric. Eng. Res.* **1984**, *30*, 245–253.
26. Shrestha, D.P.; Jetten, V.G. Modelling erosion on a daily basis, an adaptation of the MMF approach. *Int. J. Appl. Earth Obs. Geoinf.* **2018**, *64*, 117–131. https://doi.org/10.1016/j.jag.2017.09.003
27. Quijano, L.; Beguería, S.; Gaspar, L.; Navas, A. Estimating erosion rates using 137Cs measurements and WATEM/SEDEM in a Mediterranean cultivated field. *Catena* **2016**, *138*, 38–51. https://doi.org/10.1016/j.catena.2015.11.009
28. Morgan, R.P.C.; Quinton, J.N.; Smith, R.E.; Govers, G.; Poesen, J.W.A.; Auerswald, K.; Chisci, G.; Torri, D.; Styczen, M.E. The European Soil Erosion Model (EUROSEM): A dynamic approach for predicting sediment transport from fields and small catchments. *Earth Surf. Process. Landforms* **1998**, *23*, 527–544. https://doi.org/10.1002/(SICI)1096-9837(199806)23:6<527::AID-ESP868>3.0.CO;2-5
29. Boufala, M.H.; El Hmaidf, A.; Chadli, K.; Essahlaoui, A.; El Ouali, A.; Lahjouj, A. Assessment of the risk of soil erosion using RUSLE method and SWAT model at the M'dez Watershed, Middle Atlas, Morocco. In *Proceedings of the E3S Web of Conferences*, Volume 150, Les Ulis, France, 2020; p. 03014. https://doi.org/10.1051/e3sconf/202015003014
30. Heddadj, D. La lutte contre l'érosion en Algérie. *Bull. Réseau Érosion* **1997**, *17*, 168–175.
31. Remini, B. L'envasement des barrages. *Bull. Réseau Érosion* **2000**, *20*, 165–171.
32. Demmak, A. *Contribution à l'étude de l'érosion et des transports solides en Algérie*; Doctoral Thesis, Université Paris VI, Paris, France, **1982**; p. 323.
33. Touaibia, B. Problématique de l'érosion et du transport solide en Algérie septentrionale. *Sécheresse* **2010**, *21*, 333–335. doi: 10.1684/sec.2010.0271
34. Mohammadi, S.; Balouei, F.; Haji, K.; Khaledi Darvishan, A.; Karydas, C.G. Country-scale spatio-temporal monitoring of soil erosion in Iran using the G2 model. *Int. J. Digit. Earth* **2021**, *14*(8), 1019–1039. https://doi.org/10.1080/17538947.2021.1919230
35. Achite, M.; Caloiero, T.; Wałęga, A.; Krakauer, N.; Hartani, T. Analysis of the Spatiotemporal Annual Rainfall Variability in the Wadi Cheliff Basin (Algeria) over the Period 1970 to 2018. *Water* **2021**, *13*, 1477. https://doi.org/10.3390/w13111477
36. Hadour, A.; Mahé, G.; Meddi, M.; Dezileau, L. Reconstruction of the Evolution of the Hydro-Sedimentary Signal to the Sea from the Study of the Sedimentary Archives: Case of the Wadi Cheliff, Algeria. *Water* **2025**, *17*, 3378. https://doi.org/10.3390/w17233378
37. Zaibak, I.; Meddi, M. Simulating streamflow in the Cheliff Basin of west northern Algeria using the SWAT model. *J. Earth Syst. Sci.* **2022**, *131*, 25. https://doi.org/10.1007/s12040-021-01777-x
38. Toumi, S.; Meddi, M.; Mahé, G. Assessment of Water Soil Erosion by RUSLE Model Using Remote Sensing and GIS in Wadi Cheliff Basin (Algeria). In *Research Developments in Geotechnics, Geo-Informatics and Remote Sensing. CAJG 2019*; El-Askary, H., Erguler, Z.A., Karakus, M., Chaminé, H.I., Eds.; Springer: Cham, Switzerland, 2022; pp. 613–623. https://doi.org/10.1007/978-3-030-72896-0_59
39. Lin, Q.; Wang, X. Soil erosion prediction using RUSLE with GIS: A case study in Upper Chaobai River Basin of China. In *Proceedings of the IEEE International Symposium on Geoscience and Remote Sensing (IGARSS)*, Denver, CO, USA, 31 July–4 August 2006; pp. 277–280.
40. Agence Nationale des Ressources Hydrauliques (ANRH). *Accueil – Agence Nationale des Ressources Hydrauliques*. Available online: https://anrh.dz/ (accessed on 15 March 2025).
41. U.S. Geological Survey (USGS). *EarthExplorer*. Available online: https://earthexplorer.usgs.gov/ (accessed on 27 March 2025).
42. Food and Agriculture Organization of the United Nations (FAO). *Harmonized World Soil Database (Version 1.2)*. Available online: https://www.fao.org/soils-portal/data-hub/soil-maps-and-databases/harmonized-world-soil-database-v12/en/ (accessed on 05 April 2025).
43. Renard, K.G. Using monthly precipitation data to estimate the R-factor in the revised USLE. J. Hydrol. 1994, 157, 287–306. https://doi.org/10.1016/0022-1694(94)90110-4
44. Patil, R.J.; Sharma, S.K.; Tignath, S.; Sharma, A.P.M. Use of remote sensing, GIS and C++ for soil erosion assessment in the Shakkar River Basin, India. Hydrol. Sci. J. 2016, 62(2), 217–231. https://doi.org/10.1080/02626667.2016.1217413

 doi:10.20944/preprints202602.1876.v1

45. Atoma, H.; Suryabhagavan, K.V.; Balakrishnan, M. Soil erosion assessment using RUSLE model and GIS in Huluka watershed, Central Ethiopia. *Sustain. Water Resour. Manag.* **2020**, *6*, 12. https://doi.org/10.1007/s40899-020-00365-z
46. Ganasri, B.P.; Ramesh, H. Assessment of Soil Erosion by RUSLE Model Using Remote Sensing and GIS—A Case Study of Nethravathi Basin. *Geosci. Front.* **2016**, *7*, 953–961. https://doi.org/10.1016/j.gsf.2015.10.007
47. Dabral, P.; Baithuri, N.; Pandey, A. Soil Erosion Assessment in a Hilly Catchment of North Eastern India Using USLE, GIS and Remote Sensing. *Water Resour. Manag.* **2008**, *22*, 1783–1798. http://dx.doi.org/10.1007/s11269-008-9253-9
48. Naqvi, H.R.; Abdul Athick, A.S.M.; Ganaie, H.A.; Siddiqui, M.A. Soil erosion planning using sediment yield index method in the Nun Nadi watershed, India. Int. Soil Water Conserv. Res. 2015, 3(2), 86–96. https://doi.org/10.1016/j.iswcr.2015.06.007
49. Milentijević, N.; Ostojić, M.; Fekete, R.; Kalkan, K.; Ristić, D.; Bačević, N.R.; Stevanović, V.; Pantelić, M. Assessment of Soil Erosion Rates Using Revised Universal Soil Loss Equation (RUSLE) and GIS in Bačka (Serbia). *Pol. J. Environ. Stud.* **2021**, *30*(6), 5175–5184. https://doi.org/10.15244/pjoes/135617
50. Markose, V.J.; Jayappa, K.S. Soil loss estimation and prioritization of sub-watersheds of Kali River basin, Karnataka, India, using RUSLE and GIS. *Environ. Monit. Assess.* **2016**, *188*, 225. https://doi.org/10.1007/s10661-016-5218-2
51. Renard, R.; Freimund, G. Using monthly precipitation data to estimate the R factor in the Revised USLE. J. Hydrol. 1994, 157, 287–306.
52. Morgan, R.P.C. Soil Erosion and Conservation, 2nd ed.; Longman Group: Essex, UK, 1995.
53. Moore, I.D.; Burch, G.J. Physical Basis of the Length–Slope Factor in the Universal Soil Loss Equation. *Soil Sci. Soc. Am. J.* **1986**, *50*, 1294–1298. http://dx.doi.org/10.2136/sssaj1986.03615995005000050042x
54. Dutta, S. Soil erosion, sediment yield and sedimentation of reservoir: a review. *Model. Earth Syst. Environ.* **2016**, *2*, 123. https://doi.org/10.1007/s40808-016-0182-
55. Panagos, P.; Borrelli, P.; Poesen, J.; Ballabio, C.; Lugato, E.; Meusburger, K.; Montanarella, L.; Alewell, C. The new assessment of soil loss by water erosion in Europe. *Environ. Sci. Policy* **2015**, *54*, 438–447. https://doi.org/10.1016/j.envsci.2015.08.012
56. Alexandridis, T.K.; Sotiropoulou, A.M.; Bilas, G.; Karapetsas, N.; Silleos, N.G. The effects of seasonality in estimating the C-Factor of soil erosion studies. *Land. Degrad. Dev.* **2015**, *26*, 596–603.
57. Feng, Q.; Zhao, W.; Ding, J.; Fang, X.; Zhang, X. Estimation of the cover and management factor based on stratified coverage and remote sensing indices: A case study in the Loess Plateau of China. *J. Soils Sediments* **2018**, *18*, 775–790.
58. Ayalew, D.A.; Deumlich, D.; Šarapatka, B.; Doktor, D. Quantifying the Sensitivity of NDVI-Based C Factor Estimation and Potential Soil Erosion Prediction using Spaceborne Earth Observation Data. Remote Sens. **2020**, 12, 1136. https://doi.org/10.3390/rs12071136
59. Van der Knijff, J.M.; Jones, R.J.A.; Montanarella, L. *Soil Erosion Risk Assessment in Italy*; EUR 19022 EN.; European Soil Bureau, Joint Research Center of the European Commission: Ispra, Italy, 1999.
60. Pan, B.J.; Zhao, W.W.; Chen, L.D.; Zhang, Q.J.; Lü, Y.H.; Gulinck, H.; Poesen, J. Assessment of soil erosion at large watershed scale using RUSLE and GIS: a case study in the Loess Plateau of China. *Land Degrad. Dev.* **2005**, *16*, 73–85. https://doi.org/10.1002/ldr.646
61. Biswas, S.S.; Pani, P. Estimation of soil erosion using RUSLE and GIS techniques: a case study of Barakar River basin, Jharkhand, India. *Model. Earth Syst. Environ.* **2015**, *1*, 42. https://doi.org/10.1007/s40808-015-0040-3
62. Chadli, K. Estimation of soil loss using RUSLE model for Sebou watershed (Morocco). *Model. Earth Syst. Environ.* **2016**, *2*, 51. https://doi.org/10.1007/s40808-016-0105-y
63. Tarboton, D.G. A new method for the determination of flow directions and upslope areas in grid digital elevation models. Water Resour. Res. 1997, 33(2), 309–319. https://doi.org/10.1029/96WR03137
64. Moore, I.D.; Grayson, R.B.; Ladson, A.R. Digital terrain modelling: A review of hydrological, geomorphological, and biological applications. *Hydrol. Processes* **1991**, *5*(1), 3–30. https://doi.org/10.1002/hyp.3360050103

 doi:10.20944/preprints202602.1876.v1

65. Jiang, B.; Bamutaze, Y.; Pilesjö, P. Climate change and land degradation in Africa: a case study in the Mount Elgon region, Uganda. *Geo-Spatial Inf. Sci.* **2014**, *17*(1), 39–53. https://doi.org/10.1080/10095020.2014.889271
66. Meddi, M.; Toumi, S.; Assani, A.A. Spatial and temporal variability of the rainfall erosivity factor in Northern Algeria. *Arab. J. Geosci.* **2016**, *9*, 282. https://doi.org/10.1007/s12517-015-2303-8
67. Vezina, K.; Bonn, F.; Van, C.P. Agricultural land-use patterns and soil erosion vulnerability of watershed units in Vietnam's northern highlands. *Landsc. Ecol.* **2006**, *21*, 1311–1325. https://doi.org/10.1007/s10980-006-0023-x
68. Alemu, M.D.; Laekemariam, F.; Belay, S.; Teferi, E.; Hailu, A.; Mekonnen, D.; Taddesse, A.; Shiferaw, A. Modeling soil erosion for sustainable landscape management using RUSLE in the landscapes of Abaya-Chamo Sub-Basin, Ethiopia. *Model. Earth Syst. Environ.* **2025**, *11*, 171. https://doi.org/10.1007/s40808-025-02337-8
69. Saoud, M.; Meddi, M. Mapping of erosion using USLE, GIS and remote sensing in Wadi El Hachem watershed (Northern Algeria): Case study. *J. Indian Soc. Remote Sens.* **2022**, *50*, 569–581. https://doi.org/10.1007/s12524-021-01481-9
70. Panagos, P.; Ballabio, C.; Borrelli, P.; Meusburger, K.; Klik, A.; Rousseva, S.; Tadić, M.P.; Michaelides, S.; Hrabalíková, M.; Olsen, P.; Aalto, J.; Lakatos, M.; Rymszewicz, A.; Dumitrescu, A.; Beguería, S.; Alewell, C. Rainfall erosivity in Europe. *Sci. Total Environ.* **2015**, *511*, 801–814. https://doi.org/10.1016/j.scitotenv.2015.01.008
71. Bensekhria, A.; Bouhata, R. Assessment and Mapping Soil Water Erosion Using RUSLE Approach and GIS Tools: Case of Oued el-Hai Watershed, Aurès West, Northeastern of Algeria. *ISPRS Int. J. Geo-Inf.* **2022**, *11*, 84. https://doi.org/10.3390/ijgi11020084
72. Ejaz, N.; Elhag, M.; Bahrawi, J.; Zhang, L.; Gabriel, H.F.; Rahman, K.U. Soil Erosion Modelling and Accumulation Using RUSLE and Remote Sensing Techniques: Case Study Wadi Baysh, Kingdom of Saudi Arabia. *Sustainability* **2023**, *15*, 3218. https://doi.org/10.3390/su15043218
73. Hamadouche, M.A.; Daikh, F.Z.; Chrair, M.; Anteur, D.; Fekir, Y.; Driss, M. Erosion Sensitivity Mapping Using GIS-Based Multicriteria Analysis – Case Study of the Semiarid Macta Watershed, North-West of Algeria. In Recent Advances in Geo-Environmental Engineering, Geomechanics and Geotechnics, and Geohazards. CAJG 2018. Advances in Science, Technology & Innovation; Kallel, A., et al., Eds.; Springer: Cham, Switzerland, 2019; pp. 1051–1060. https://doi.org/10.1007/978-3-030-01665-4_110
74. Rashid, M.; Haider, S.; Rizwan, A.; Naseer, M.W.; Aslam, M.F.; Hamza, M.; Nadeem, A.; Abbasi, H.K.J.; Tariq, M.A.U.R. Mitigating soil erosion in arid landscapes: Integrating RUSLE and geospatial analysis for sustainable land management. Environ. Chall. 2025, 20, 101210. https://doi.org/10.1016/j.envc.2025.101210
75. Zeghmar, A.; Marouf, N.; Mokhtari, E. Assessment of soil erosion using the GIS-based erosion potential method in the Kebir Rhumel Watershed, Northeast Algeria. J. Water Land Dev. 2022, No. 52, 133–144. https://doi.org/10.24425/jwld.2022.140383
76. Cherif, K.; Yahia, N.; Bilal, B.; Meziane, T.; Zekraoui, L.; Meziane, A.; Bencherif, H.; Belaidi, N.; Bensebaa, Z. Erosion potential model-based ANN-MLP for the spatiotemporal modeling of soil erosion in Wadi Saida watershed. *Model. Earth Syst. Environ.* **2023**, *9*, 3095–3117. https://doi.org/10.1007/s40808-022-01657-3
77. Zerouali, B.; Ayek, A.A.E.; Bailek, N.; et al. RUSLE Model Insights for Soil Conservation and Sustainable Land Use in Semiarid Environments. Euro-Mediterr. J. Environ. Integr. **2025**, *10*, 853–876. https://doi.org/10.1007/s41207-024-00664-3
78. Toumi, S.; Meddi, M. Integrated RUSLE–GIS–RS analysis of soil erosion and sediment yield in the Wadi Cheliff Basin, Algeria. *Appl. Geomat.* **2026**, *18*, 40. https://doi.org/10.1007/s12518-026-00701-6
79. Pantazis, C.; Nastos, P. Comparing Direct Field Measurements of Soil Erosion with RUSLE Model Estimates in Mediterranean Olive Orchards. *Environ. Earth Sci. Proc.* **2025**, *35*, 75. https://doi.org/10.3390/eesp2025035075
80. Menghis, T.B.; Zdruli, P.; Dobos, E. A GIS-Based Approach to Soil Erosion Risk Assessment Using RUSLE: The Case of the Mai Nefhi Watershed, Barka River Basin, Eritrea. *Earth* **2025**, *6*, 58. https://doi.org/10.3390/earth6020058

 doi:10.20944/preprints202602.1876.v1

81. Fadl, M.E.; Zekari, M.; Labad, R.; et al. Integrating RUSLE, AHP, GIS, and Cloud-Based Geospatial Analysis for Soil Erosion Assessment under Mediterranean Conditions. *Sci. Rep.* **2025**, *15*, 38494. https://doi.org/10.1038/s41598-025-22503-3
82. Abdo, H.G.; Almohamad, H.; Al Dughairi, A.A.; Al-Mutiry, M. Quantifying the Water Soil Erosion Rate Using RUSLE, GIS, and RS Approach for Al-Qshish River Basin, Lattakia, Syria. Geofizika 2022, 39(2), 12. https://doi.org/10.15233/gfz.2022.39.12
83. Nieto, C.E.; Martínez-Graña, A.M.; Merchán, L. Soil Erosion Risk Analysis in the Ría de Arosa (Pontevedra, Spain) Using the RUSLE and GIS Techniques. *Forests* **2024**, *15*, 1481. https://doi.org/10.3390/f15091481